LITHOS 404-405 (2021) 106463

Contents lists available at ScienceDirect

LITHOS

journal homepage: www.elsevier.com/locate/lithos

Research Article

Ordovician to Devonian granitic plutons in the Hangay Range, Central Mongolia: Petrogenesis and insights into the Paleozoic tectonic evolution of the westernmost Mongol-Okhotsk Orogen

Jiaqi Ling [a,b,c], Pengfei Li [a,b,*], Chao Yuan [a,b], Min Sun [d], Yunying Zhang [d], Tserendash Narantsetseg [e], Xiangsong Wang [d], Yingde Jiang [a,b], Wanwan Hu [a,b,c]

[a] State Key Laboratory of Isotope Geochemistry, Guangzhou Institute of Geochemistry, Chinese Academy of Sciences, Guangzhou 510460, China
[b] CAS Center for Excellence in Deep Earth Science, Guangzhou 510640, China
[c] University of Chinese Academy of Sciences, Beijing 10049, China
[d] Department of Earth Sciences, the University of Hong Kong, Pokfulam Road, Hong Kong, China
[e] Institute of Geology of Mongolian Academy of Sciences, Ulaanbaatar 15160, Mongolia

ARTICLE INFO

Keywords:
Central Asian Orogenic Belt
Mongol-Okhotsk orogen
Hangay range
Granitoids
Petrogenesis
Accretionary orogen

ABSTRACT

The pre-Mesozoic magmatic and tectonic evolution in the Mongol-Okhotsk Orogen has been poorly understood. Here we conducted geochronological and geochemical studies on five Paleozoic granitic plutons in the westernmost Mongol-Okhotsk Orogen (Hangay Range), with an aim to understand their petrogenesis and roles in the Paleozoic tectonic evolution of the Mongol-Okhotsk Orogen. Our results demonstrate that two K-feldspar granites yield Ordovician to Silurian zircon U-Pb ages of 469 ± 3 Ma and 440 ± 3 Ma, and three monzogranites give Devonian zircon U-Pb ages (416 ± 4 Ma, 416 ± 4 Ma and 398 ± 4 Ma). Geochemical data show that all plutons in this study have high SiO_2 (65.8–77.9 wt%) and total alkali (6.3–8.9 wt%) contents, and are enriched in large-ion lithophile elements (LILEs, e.g. Rb, Th and K) and depleted in high-field-strength elements (HFSEs, e.g. Nb, Ta and Ti). Furthermore, the Ordovician K-feldspar granite has the characteristics of A_2-type granitic rocks with high 10000*Ga/Al (3.4–3.6), while Silurian to Devonian granitic plutons belong to I-type granitoids with low A/CNK values (0.8–1.1). The low Na_2O/K_2O ratios (0.5–0.7) of the Ordovician and Silurian K-feldspar granites suggest that they were generated by partial melting of medium-to-high K basaltic rocks. Three Devonian monzogranites with high Na_2O/K_2O ratios (1.1–1.7) have an origin of low-K basaltic rocks. Five Ordovician to Devonian granitic plutons have relatively low $\varepsilon_{Nd}(t)$ values (−4.7 to +0.5) and variable zircon $\varepsilon_{Hf}(t)$ values from −2.6 to +5.5, which plot between the evolutional lines of depleted mantle and the Precambrian basement rocks of microcontinents, and are interpreted to result from partial melting of the relatively juvenile mafic rocks that were underplated in response to the Ediacaran to Cambrian subduction. Given the development of accretionary complex in the westernmost Mongol-Okhotsk Orogen during the Paleozoic, we interpreted these plutons to be formed in a supra-subduction zone associated with the consumption of the Mongol-Okhotsk oceanic plate. In particular, the Ordovician K-feldspar granite intruded into the Cambrian to Ordovician accretionary complex, which, together with its A_2-type characteristics, suggests an episode of slab rollback at ~469 Ma.

1. Introduction

The accretion mechanism of the Central Asian Orogenic Belt (CAOB) has attracted widespread attentions in the past decades given its crucial role in understanding the Phanerozoic continental growth (Jiang et al., 2011; Şengör et al., 1993; Windley et al., 2007; Xiao et al., 2015). Various tectonic models have been proposed to explain the evolution of the CAOB, with two end members of the progressive development of a single arc system (Şengör et al., 1993), and the amalgamation of multiple arc systems (Windley et al., 2007; Xiao et al., 2015). The former emphasizes the prolonged evolution of a single arc system (the Kipchak-Tuva-Mongol arc), while the latter is characterized by the coeval

* Corresponding author at: State Key Laboratory of Isotope Geochemistry, Guangzhou Institute of Geochemistry, Chinese Academy of Sciences, Guangzhou 510460, China.
E-mail addresses: pengfeili@gig.ac.cn, pengfeili2013@gmail.com (P. Li).

https://doi.org/10.1016/j.lithos.2021.106463
Received 27 June 2021; Received in revised form 5 September 2021; Accepted 6 September 2021
Available online 8 September 2021

development of multiple arc systems. In order to better evaluate the role of the above mechanisms, it is important firstly to unravel the spatial and temporal evolution of magmatism within the CAOB.

The Mongol-Okhotsk Orogen in the eastern CAOB extends from the Hangay Range (central Mongolia) to the Okhotsk Sea (Fig. 1a). Its Mesozoic tectonic evolution is generally considered to be associated with the subduction of the Mongol-Okhotsk oceanic plate (Donskaya et al., 2013; van der Voo et al., 2015). However, pre-Mesozoic tectonic evolution has been poorly understood. Şengör et al. (1993) considered that the subduction of the Mongol-Okhotsk oceanic plate lasted from the Ediacaran to Mesozoic on a basis of the recognized accretionary complex in this period. Such an interpretation suffers from the scarcity of geochronological and geochemical constraints from the pre-Mesozoic magmatic rocks along the whole Mongol-Okhotsk Orogen, and thus it remains enigmatic whether the accretionary complex was accompanied by the development of a magmatic arc in the Mongol-Okhotsk Orogen.

In the westernmost Mongol-Okhotsk Orogen (Hangay Range; Fig. 1c), the Bayanhongor ophiolite has been dated at ~655–636 Ma (Jian et al., 2010), indicating the existence of the oceanic basin in the late Neoproterozoic. Ediacaran to Cambrian igneous rocks in this region are characterized by enrichment in LILEs (e.g. Rb, Th and K) and depletion in HFSEs (e.g. Nb, Ta and Ti), which, together with the coeval development of the accretionary complex, suggests an Andean-type subduction system during this period (Demoux et al., 2009; Jahn et al., 2004; Zhang et al., 2015b). However, it remains enigmatic how this subduction system subsequently evolved in the Paleozoic. Some authors proposed an Ordovician to Devonian collisional event to terminate the subduction, following the docking of an "unknown microcontinent" beneath the Hangay-Hentey complex (Fig. 1c; Buchan et al., 2002; Osozawa et al., 2008). However, there is no evidence for the existence of such an "unknown microcontinent", and the Hangay-Hentey complex has been alternatively interpreted to represent an accretionary complex (Erdenesaihan et al., 2013; Ruppen et al., 2014; Tsukada et al., 2013). Therefore, a re-investigation on the Paleozoic tectonic evolution of the westernmost Mongol-Okhotsk Orogen is imperative.

In this work, we conducted geochronological and geochemical studies on five Ordovician to Devonian granitic plutons in the westernmost Mongol-Okhotsk Orogen (Hangay Range), with an aim to investigate their petrogenesis and roles in the Paleozoic tectonic evolution of the Mongol-Okhotsk Orogen. Our results show that there was no Ordovician to Devonian magmatic gap in the westernmost Mongol-Okhotsk Orogen, and the subduction was likely continuous during this period.

2. Geological setting

The Mongolian segment of the CAOB can be tectonically divided into the northern and southern domains by the Main Mongolian Lineament (Fig. 1c; Badarch et al., 2002). The former is dominated by Precambrian microcontinental blocks and island arcs, while the latter is mainly occupied by late Paleozoic island arc systems (Badarch et al., 2002;

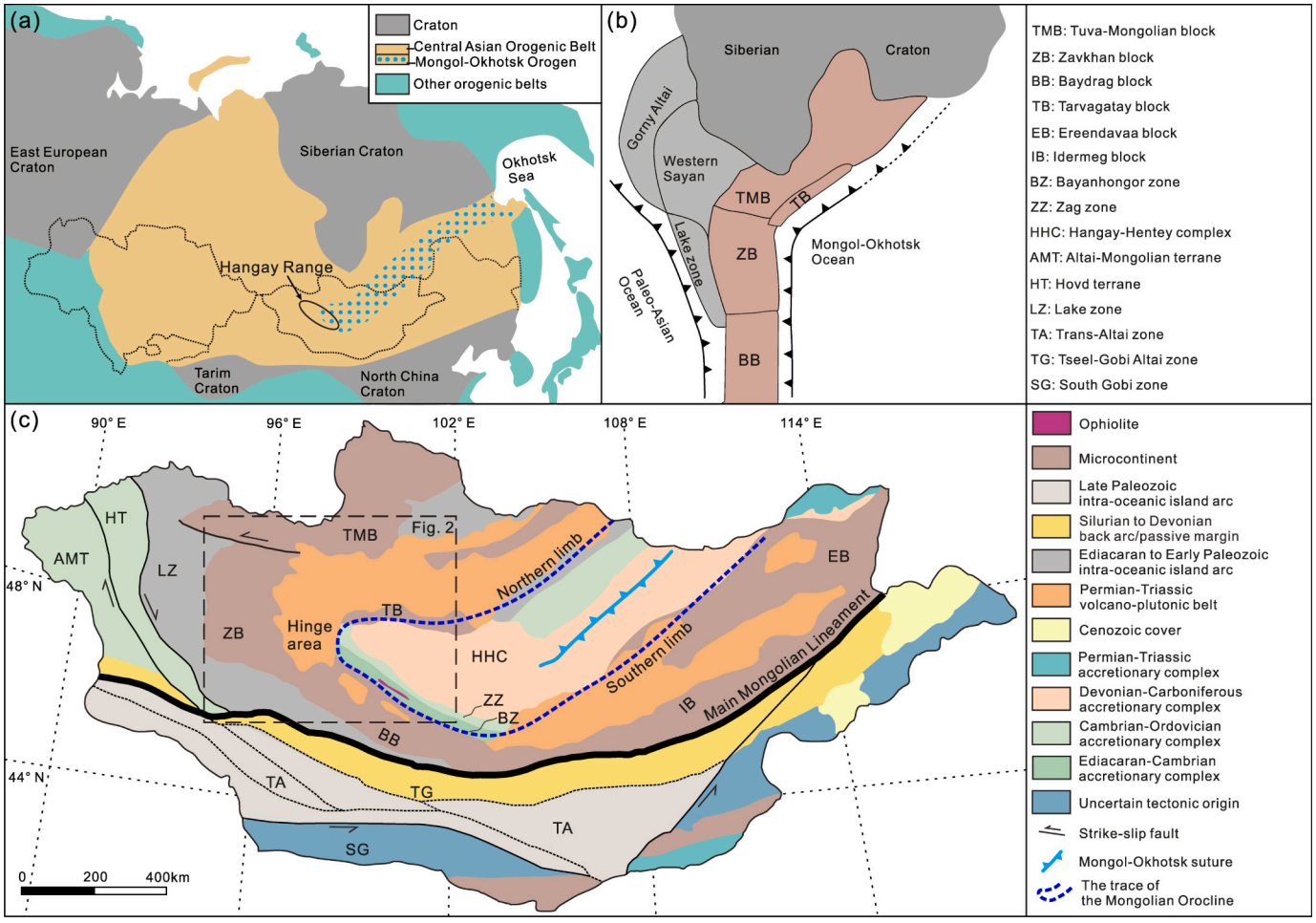

Fig. 1. (a) A simplified tectonic map with major tectonic units around the Central Asian Orogenic Belt (CAOB) (modified from Şengör et al., 1993). (b) A schematic reconstruction map of the northern CAOB in the early Paleozoic (modified from Delvaux et al., 1995). (c) The tectonic map of Mongolia (modified from Badarch et al., 2002; Li et al., 2022).

Lehmann et al., 2010). The Mongol-Okhotsk Orogen is located in the northern domain, and extends over 3000 km from central Mongolia (Hangay Range) to the gulf of Okhotsk Sea (Fig. 1a; Zorin et al., 1993). It shows an orogenic curvature in a map view (Mongolian Orocline), with the hinge zone located in the Hangay Range (Fig. 1; Şengör et al., 1993; Li et al., 2022).

In the hinge area of the Mongolian Orocline, a series of micro-continental blocks of Tuva-Mongolian, Tarvagatay, Zavkhan and Baydrag are aligned around the orocline (Figs. 1c and 2). They were considered to represent a continental ribbon (e.g. Lehmann et al., 2010) with the northern segment (current coordinate) accreted to the Siberian margin at ~630–610 Ma (Gladkochub et al., 2019; Li et al., 2019). The Tuva-Mongolian block in the north comprises Archean to Paleoproterozoic granulite, amphibolite and gneiss, which are overlain by Early Neoproterozoic volcanic rocks, clastic rocks and carbonates (Kravchinsky et al., 2010). The Tarvagatay block, which is located to the south of the Tuva-Mongolian block, mainly consists of Archean to Paleoproterozoic gneiss, amphibolite and schist (Badarch et al., 2002; Kozakov et al., 2011; Kröner et al., 2014). These rocks are overlain by Neoproterozoic to Early Cambrian limestone and Devonian-Carboniferous sandstone and conglomerate (Badarch et al., 2002). Farther southwest, the Zavkhan block is characterized by the Proterozoic basement (Bold et al., 2016; Kozakov et al., 2014), which is covered by Neoproterozoic volcanic rocks, clastic rocks and carbonates (Kozakov et al., 2014, 2015). The Baydrag block in the south is mainly composed of Archean to Proterozoic tonalitic to granitic gneiss and granulite that are unconformably overlain by Neoproterozoic sandstone and Devonian to Permian volcaniclastic rocks (Demoux et al., 2009; Kröner et al., 2017).

The core area of the Mongolian Orocline in the Hangay Range is mainly occupied by the Bayanhongor zone, the Zag zone and the Hangay-Hentey complex (Fig. 2), which were interpreted to develop within an accretionary wedge (Şengör et al., 2018; Şengör et al., 1993). The Bayanhongor zone in the west is represented by a pile of Neoproterozoic to Cambrian tectonic mélange with ~647–630 Ma ophiolite incorporated (Buchan et al., 2001; Jian et al., 2010). Farther east, the Zag zone mainly contains the Cambrian and Ordovician pelitic and psammitic schists (Buchan et al., 2001). The Hangay-Hentey complex predominantly consists of the Devonian to Carboniferous turbidite sequence, which is mixed with the ocean island basalt, the radiolarian chert, and the oceanic plate stratigraphy (Erdenesaihan et al., 2013; Tsukada et al., 2013).

Permian to Triassic magmatic rocks widely occur around the Mongolian Orocline (Fig. 1c), which were interpreted to be associated with the subduction of the Mongol-Okhotsk oceanic plate (Jahn et al., 2004; Yarmolyuk et al., 2019). Pre-Permian magmatic rocks were also recognized in both limb and hinge areas of the Mongolian Orocline (Fig. 2). Donskaya et al. (2013) reported late Paleozoic arc-related magmatic rocks along the northern limb of the orocline, and suggested that the subduction of the Mongol-Okhotsk oceanic plate beneath the northern limb of the orocline was active in this period. Along the southern limb of the orocline, the Carboniferous adakitic magmatism had been recognized, and was interpreted to result from the subduction of the Mongol-Okhotsk oceanic plate (Sun et al., 2013). In the hinge area of the Mongolian Orocline (Hangay Range; Fig. 2), the Ediacaran to Cambrian intrusions show arc-like features (enrichment in LILEs and depletion in HFSEs), indicating that the subduction was active during this period (Demoux et al., 2009; Jahn et al., 2004; Zhang et al., 2015b).

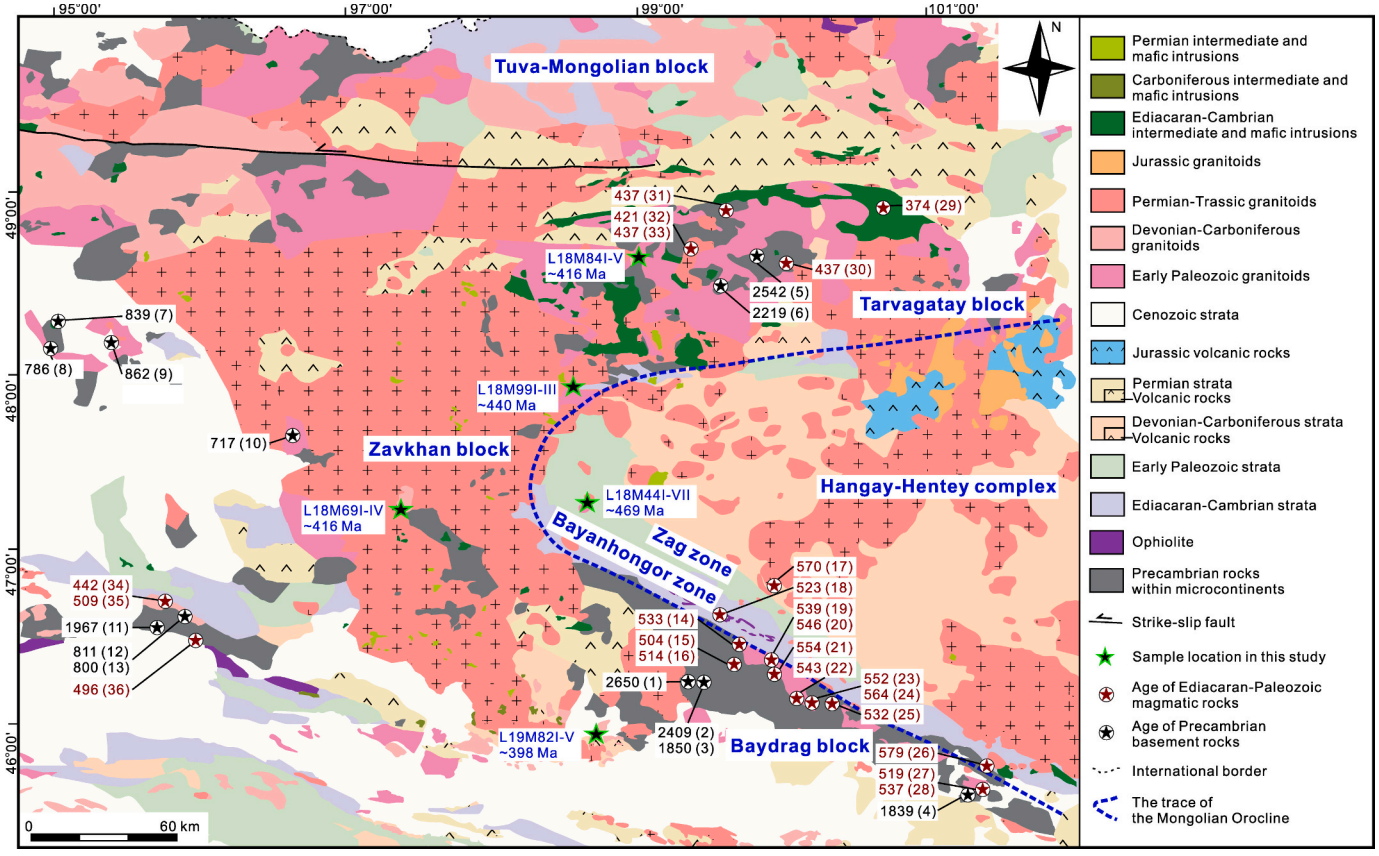

Fig. 2. Geological map in the area of the Hangay Range (central Mongolia) (based on 1:500, 000 geological map published in 1990). See the figure location in Fig. 1c. The age data and related references are listed in Table S1.

3. Sample description and analytical methods

3.1. Sample description

In this study, we collected twenty-four samples from five different granitic plutons in the westernmost Mongol-Okhotsk Orogen (Hangay Range in central Mongolia; Fig. 2). The geochronological and geochemical analyses were conducted for these samples with an aim to constrain their petrogenesis and geodynamic setting.

Two K-feldspar granite plutons are targeted for sampling. Samples L18M44I-VII are from a pluton that intruded into the Zag zone, while samples L18M99I-III are from a pluton that occurs along the eastern margin of the Zavkhan block (Fig. 2). The former mainly contains medium-grained K-feldspar (~60 vol%), plagioclase (~10 vol%), quartz (~25 vol%), and biotite (~5 vol%) (Fig. 3a). The latter is composed of K-feldspar (~50 vol%), plagioclase (~20 vol%), quartz (~25 vol%), and minor magnetite (Fig. 3b).

Three additional plutons for sampling are monzogranites. Samples L18M84I-V are from a monzogranite within the Tarvagatay block (Fig. 2), and are characterized by a mineral assemblage of plagioclase (~35 vol%), K-feldspar (~30 vol%), quartz (~15 vol%), hornblende (~10 vol%), biotite (~5 vol%) and minor magnetite (Fig. 3c). Samples L18M69I-IV are from a pluton within the Zavkhan block (Fig. 2), and consist of K-feldspar (~40 vol%), plagioclase (~30 vol%), quartz (~20 vol%), biotite (~5 vol%), and magnetite (~5 vol%) (Fig. 3d). Minor alteration is observed for plagioclase in these samples. Samples L19M82I-V are from a pluton within the Baydrag block, and show a mineral assemblage of K-feldspar (~35 vol%), plagioclase (~40 vol%), quartz (~20 vol%), and biotite (~5 vol%) (Fig. 3e).

3.2. Analytical methods

3.2.1. U-Pb geochronology

Zircon grains were separated using traditional heavy liquid and

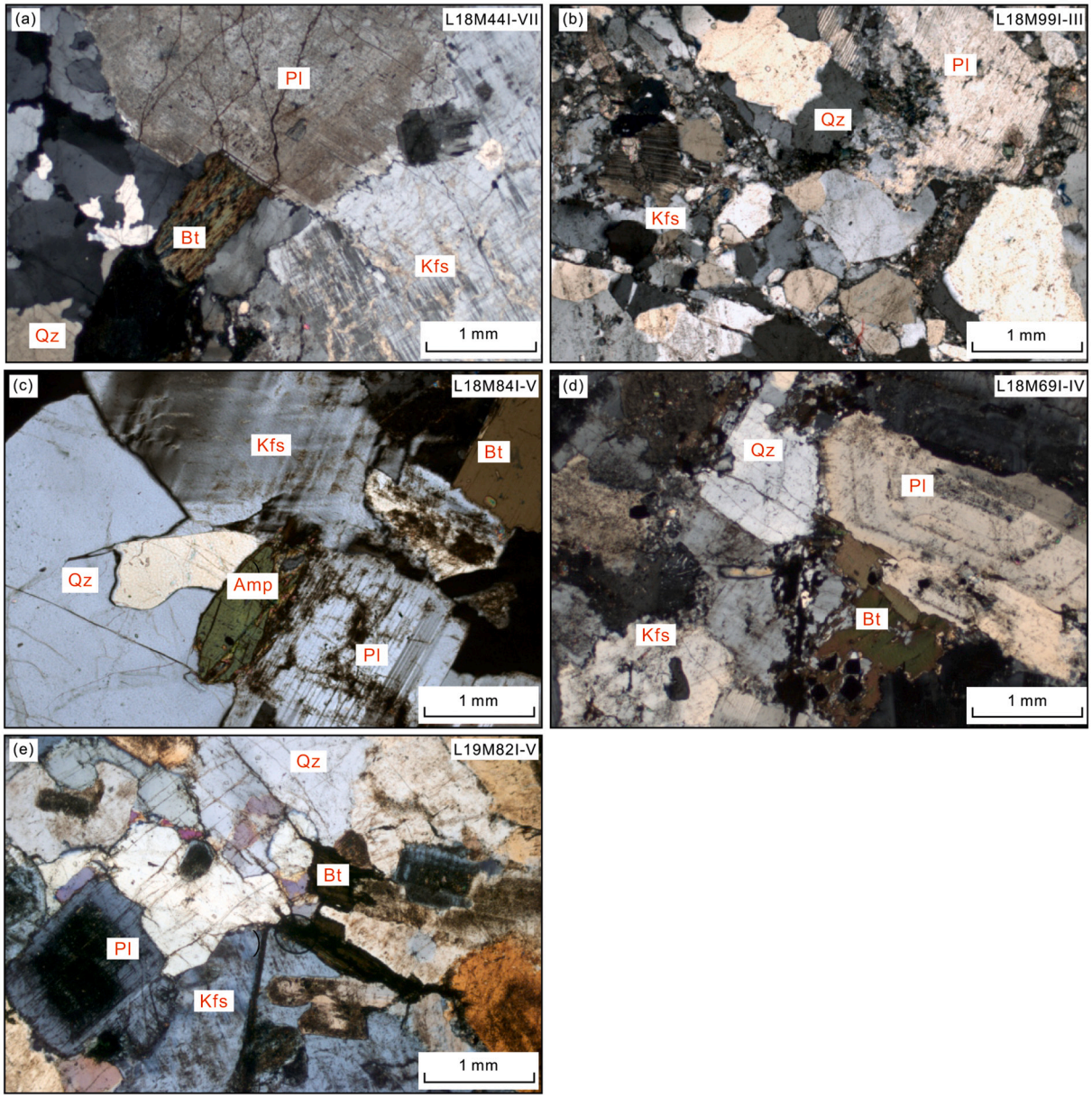

Fig. 3. Photomicrographs of granitic plutons, showing major mineral assemblages of samples in this study. (a) The Ordovician K-feldspar granite (~469 Ma); (b) The Silurian K-feldspar granite (~440 Ma); (c-e) The Devonian monzogranites (~416–398 Ma). Mineral abbreviations: Amp, amphibole; Bt, biotite; Pl, plagioclase; Kfs, K-feldspar; Qz, quartz.

magnetic techniques, and were mounted in epoxy resin. Cathodoluminescence (CL) images were obtained to observe the internal structures of zircons and to target the analytical spots. The U-Pb dating of zircons was conducted by LA-ICP-MS at the Key Laboratory of Mineralogy and Metallogeny, Guangzhou Institute of Geochemistry, Chinese Academy of Sciences. The size and frequency of the laser was set to 29 μm and 6 Hz, respectively. Helium gas was used to carry the ablated sample aerosol, which was mixed with argon and nitrogen gas to enhance analytical sensitivity. The aerosol finally flowed into ICP to conduct analysis. Zircon 91500 and NIST 610 were used as external standards for U-Pb isotopic and elemental analyses, respectively. ICPMSDataCal 10.9 was used to carry out off-line selection of analyzed signals, and to handle time-drift correction and quantitative calibration for U-Pb analysis (Liu et al., 2008). Isoplot 4.15 was used to plot Concordia diagrams and to calculate the weighted mean ages (Ludwig, 2003).

3.2.2. Whole-rock geochemistry

Whole-rock geochemistry analyses were conducted in two laboratories. The first batch of samples (L18M44I-VII, L18M99I-III, L18M84I-V and L18M69I-IV) was analyzed at the State Key Laboratory of Isotope Geochemistry, Guangzhou Institute of Geochemistry, Chinese Academy of Sciences (SKLIG GIG CAS). Major elements were analyzed by X-ray fluorescence (XRF). The detailed operation is described in Li et al. (2006). The analytical precision for major elements was between 1% and 5%. Trace elements were analyzed by Thermo inductively coupled plasma mass spectrometry (iCAP Qc). The detailed analytical processes can be found in Li et al. (2002). The elemental concentrations were corrected by USGS rock standards (SARM-4, SY4, BHVO-2, W-2a, AGV-1) and Chinese national rock standards (GSR-1, GSR-2, GSR-3, GSD-9, GSD-10, GSD-12). The analytical precision for trace elements was generally better than 5%.

The second batch of samples (L19M82I-V) was analyzed at the Wuhan Samplesolution Analytical Technology Co., Ltd., Wuhan, China. Major elements were analyzed on XRF (Primus II, Rigaku, Japan), with the analyzed procedure described in Liu et al. (2008). The analytical precision for major elements was generally better than 2%. Trace elements were conducted on Agilent 7700e ICP-MS. Detailed analytical processes are documented in Liu et al. (2008). The rock standards of AGV-2, BHVO-2 and RGM-2 were used to calibrate the trace elemental concentrations. The analytical precision for trace elements was generally better than 5%.

3.2.3. Sr-Nd isotopes

Whole-rock Sr and Nd isotopes for all samples were analyzed by Neptune Plus MC-ICP-MS (Thermo Fisher Scientific, Dreieich, Germany) at the Wuhan Sample Solution Analytical Technology Co., Ltd., Wuhan, China. 50–100 mg of powder was put in a Teflon bomb, and 1–3 ml of HNO3 and HF were slowly added. Afterwards, the Teflon bomb was put in an oven, which was heated to 190 °C over 24 h. The Teflon bombs were evaporated to dryness after cooling. 1 ml of HNO_3 was added and evaporated to dryness. 1.5 ml of HCl was added in the evaporated sample. The sample was processed by centrifuge. Sr fractions were separated with an ion-exchange column of AG50W resin after centrifuge. Nd fractions were further separated by ion-exchange columns of LN resins. Finally, Sr and Nd isotopes were collected for mass-spectrometric measurement.

In this study, Sr isotopic standard (NBS SRM 987) was applied to estimate the instrumental reproducibility and accuracy. The measured $^{87}Sr/^{86}Sr$ ratio of the NBS SRM 987 is 0.710243 ± 5 (2σ, n = 14), compatible with the reported values (0.710241 ± 12; Thirlwall, 1991). In addition, two Nd isotopic standards (Jndi-1 and GSB) were also applied to evaluate the instrumental reproducibility and accuracy during the analysis of the samples. The $^{143}Nd/^{144}Nd$ ratio of the Jndi-1 is 0.512116 ± 9 (2σ, n = 7), which is similar to the recommended values (0.512115 ± 7, Tanaka et al., 2000). The measured $^{143}Nd/^{144}Nd$ ratio of the GSB is 0.512440 ± 5 (2σ, n = 9), compatible with the reported values (0.512439 ± 10; Li et al., 2017).

3.2.4. Zircon Hf isotope

Zircon Hf isotopic composition was analyzed by the Neptune Plus MC-ICP-MS (Thermo Scientific) at the SKLIG GIG CAS, connected with a RESOlution M-50193 nm laser ablation system (Resonetics). The diameter and frequency of the laser were set to 45 μm and 6 Hz, respectively. The laser energy density of 4 Jcm^{-2} was applied to ablate zircons. Helium was used as the carrier gas to transport ablating materials. The detailed analytical method is described by Wu et al. (2006). ^{173}Yb and ^{175}Lu were used to correct the isobaric interference of ^{176}Yb and ^{176}Lu on ^{176}Hf. The recommended values of $^{176}Yb/^{173}Yb$ and $^{176}Lu/^{175}Lu$ used for the correction are 0.79381 (Segal et al., 2003) and 0.02656 (Wu et al., 2006), respectively. The detailed data reduction procedure can be referred to Zhang et al. (2015a). The chondritic values of $^{176}Hf/^{177}Hf$ (0.282772) and $^{176}Lu/^{177}Hf$ (0.0332), reported by Blichert-Toft and Albarede (1997), were used to calculate the $\varepsilon_{Hf}(t)$ values. The present-day depleted mantle values ($^{176}Hf/^{177}Hf$ = 0.283250 and $^{176}Lu/^{177}Hf$ = 0.0384, Griffin et al., 2000) were used to calculate the single-stage Hf model ages (T_{DM1}). Two-stage model ages (T_{DM2}) were calculated by using the mean $f_{Lu/Hf}$ value of −0.34 for the lower crust (Amelin et al., 1999) and 0.16 for the depleted mantle (Griffin et al., 2002).

4. Results

U-Pb zircon ages for five samples are presented in Table S2. Whole rock geochemical results for twenty-four granitic samples are presented in Table S3. Whole rock Sr-Nd and in-situ zircon Hf isotopic data are listed in Tables S4 and S5, respectively.

4.1. U-Pb geochronology

Representative CL images of the analyzed zircons are presented in Fig. 4. We analyzed twenty zircon grains for each sample, and data filtering for valid ages is illustrated in Table S2. Zircons from five samples are commonly 120 μm long and have length/width ratios of 2:1 to 3:1. These zircons have moderate to high Th/U ratios (0.2–1.4), which, together with their subhedral features and oscillatory zoning (Fig. 4a-e), suggests a magmatic origin. $^{206}Pb/^{238}U$ ages are used for the zircon age calculation given that our samples are younger than 1000 Ma (Nemchin and Cawood, 2005).

We obtain eighteen valid zircon ages for the K-feldspar granite sample (L18M44V). Sixteen of them yield a weighted mean $^{206}Pb/^{238}U$ age of 469 ± 3 Ma (n = 16, MSWD = 1.5), which is interpreted to be the crystallization age of this sample (Fig. 5a and b). The other two older $^{206}Pb/^{238}U$ ages of 531 Ma and 490 Ma are interpreted to represent ages of inherited zircons.

Sample L18M99II of the K-feldspar granite is characterized by fifteen valid zircon ages, based on which we calculated a Silurian weighted mean $^{206}Pb/^{238}U$ age of 440 ± 3 Ma (n = 15, MSWD = 1.6; Fig. 5c and d). This age represents the crystallization time of sample L18M99II.

Three monzogranite samples (L18M84IV, L18M69I and L19M82I) yield Devonian ages. Sixteen zircons from sample L18M84IV show $^{206}Pb/^{238}U$ ages between 405 Ma and 426 Ma (Fig. 5e and f), with a weighted mean of 416 ± 4 Ma (n = 16, MSWD = 1.7) that is interpreted to be the crystallization age of sample L18M84IV. One additional zircon yields an older $^{206}Pb/^{238}U$ age of 446 Ma, possibly having an inherited origin. As for sample L18M69I, $^{206}Pb/^{238}U$ ages for twelve zircons range from 407 Ma to 427 Ma, with a weighted mean age of 416 ± 4 Ma (n = 12, MSWD = 1.6) that is interpreted as the crystallization age of sample L18M69I (Fig. 5g and h). One additional zircon gives an older age of 483 Ma, which was possibly inherited from the magma source or captured from the country rocks. Fourteen valid zircon ages for sample L19M82I were obtained. One of them with older $^{206}Pb/^{238}U$ age (445 Ma), is

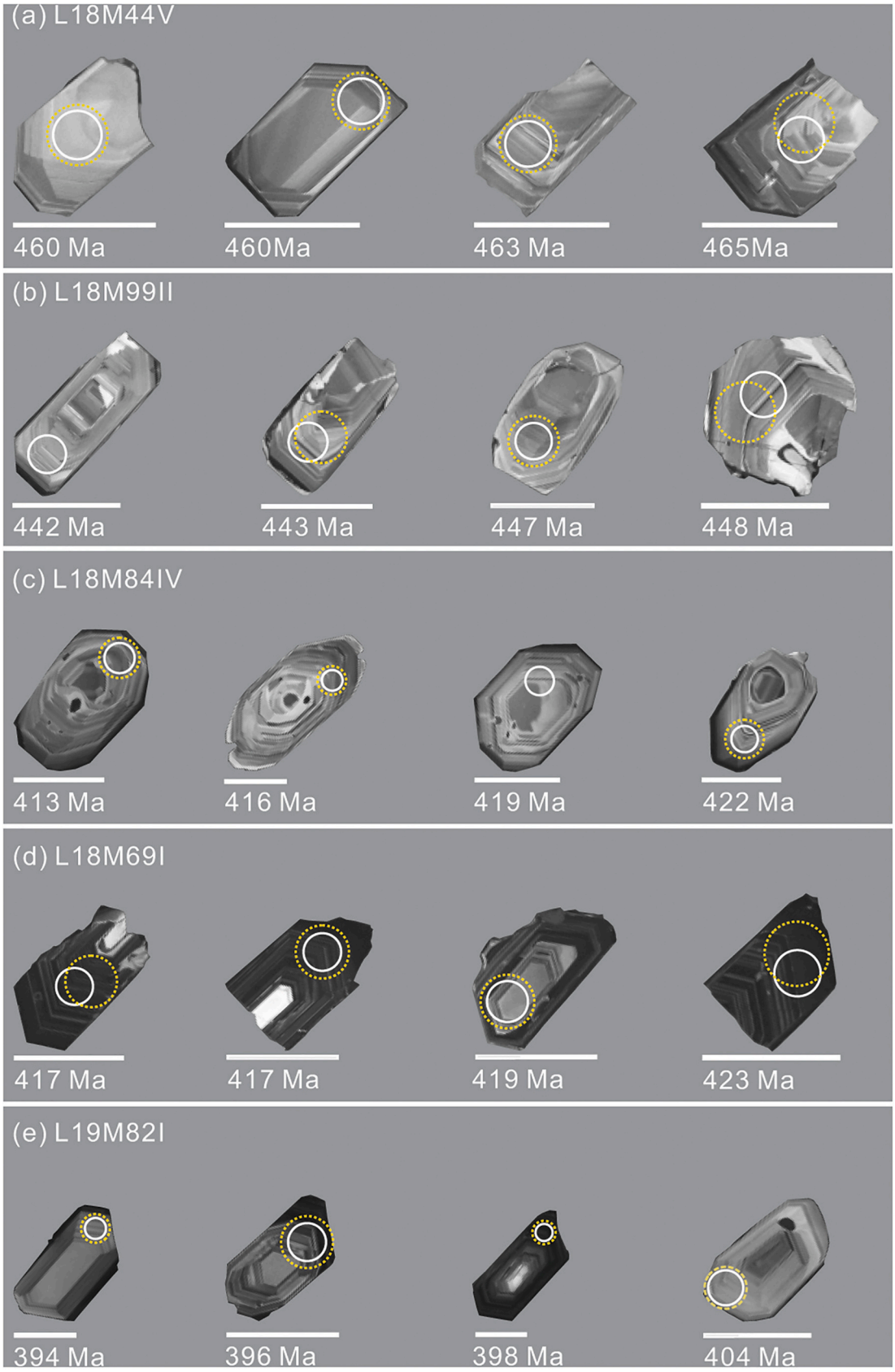

Fig. 4. CL images of representative zircons from granitic plutons in this study. White circles show the location of U-Pb analyses, while yellow circles indicate the location of Hf isotopic analyses. (For interpretation of the references to colour in this figure legend, the reader is referred to the web version of this article.)

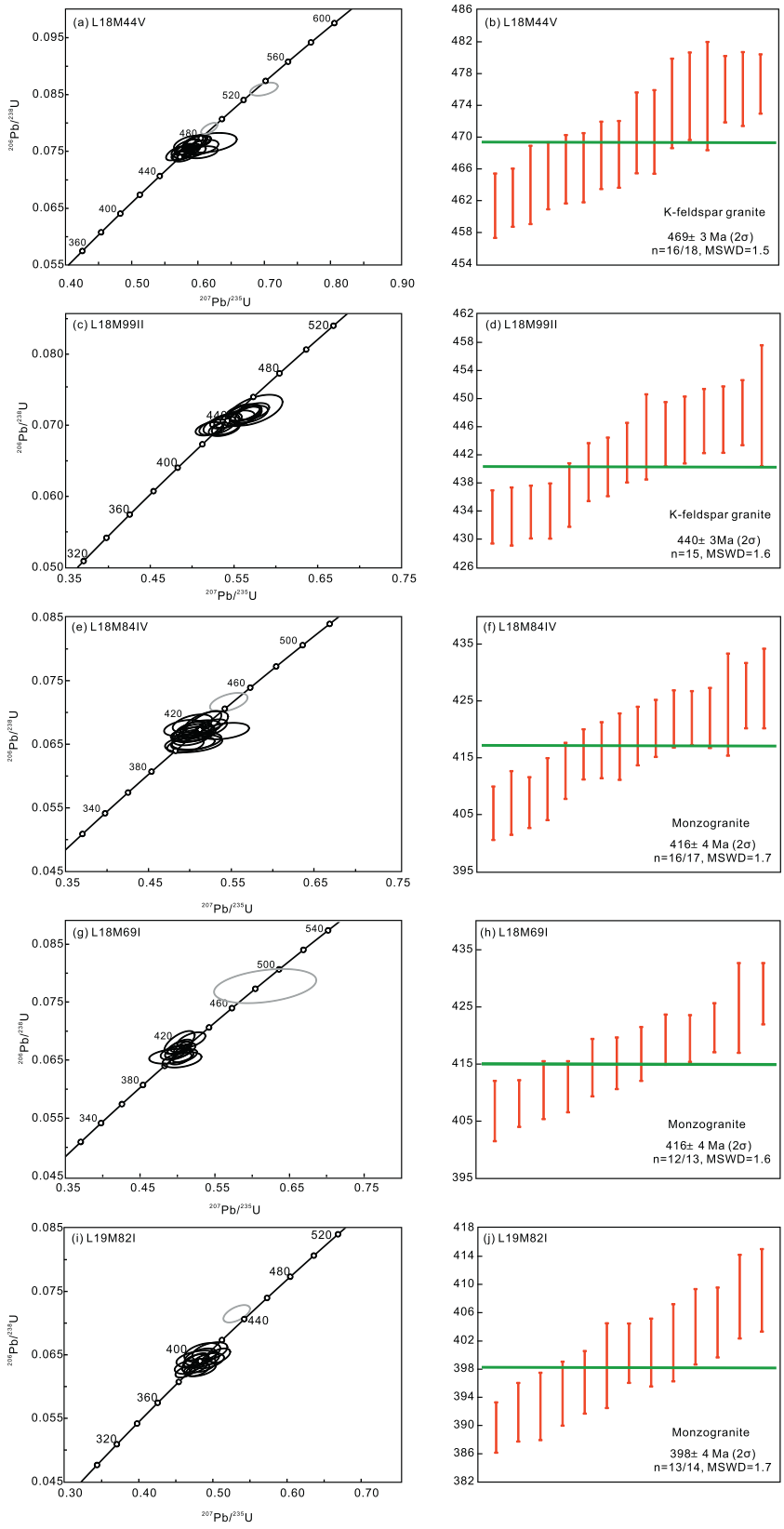

Fig. 5. Zircon U-Pb Concordia and weighted mean age diagrams, in which valid data are plotted (see valid age data in Table S2). The gray ellipses represent the age of inherited zircons in the Concordia diagrams.

interpreted to have an inherited origin. Thirteen zircons yield a weighted mean $^{206}Pb/^{238}U$ age of 398 ± 4 Ma (n = 13, MSWD = 1.7) that is interpreted to be the crystallization age of sample L19M82I (Fig. 5i and j).

4.2. Whole-rock geochemistry

The Ordovician K-feldspar granite (samples L18M44I-VII) has high SiO_2 (73.5–75.0 wt%), low Al_2O_3 (12.7–13.3 wt%) and MgO (~0.33 wt %) contents, classified as granite in the TAS diagram (Fig. 6a). The high K_2O values (4.8–5.2 wt%) of this pluton indicate the high-K calc-alkaline characteristics (Fig. 6b). In addition, the Ordovician K-feldspar granite shows metaluminous characteristics with A/CNK from 1.0 to 1.1 (Fig. 6c). The Chondrite-normalized rare earth elements (REE) show enrichment in light REEs (LREEs), and strongly negative Eu anomalies with δEu = 0.2 (Fig. 7a). On the primitive mantle (PM) normalized trace element variation diagram, the Ordovician K-feldspar granite shows significantly negative Ba, Nb, Ta, P and Ti anomalies and positive Rb, Th and K anomalies (Fig. 7b). Specifically, the granite possesses low Sr (39.9–46.1 ppm), high Rb (172.9–194.9 ppm) and Y (56.3–89.0 ppm) contents.

The Silurian K-feldspar granite (samples L18M99I-III) exhibits high SiO_2 (77.5–77.9 wt%), and low Al_2O_3 and $Fe_2O_3^T$. Similar to the Ordovician K-feldspar granite, this granite is also plotted into the granite field in the TAS diagram (Fig. 6a), and belongs to the high-K calc-alkaline series (Fig. 6b). The Silurian K-feldspar granite shows metaluminous characteristics because this granite possesses low A/NCK values (0.8–0.9; Fig. 6c). The trace elements of the Silurian K-feldspar granite are characterized by strong REE fractionation ($(La/Yb)_N$ = 11.5–38.7) and significantly negative Eu anomalies (~0.2) in the chondrite-normalized REE diagrams (Fig. 7c). In the primitive mantle (PM) normalized spider diagram, the Silurian K-feldspar granite shows significantly negative Nb, Ta, P and Ti anomalies and enrichment of Rb, Ba, Zr and Hf (Fig. 7d). Additionally, the Silurian K-feldspar granite has low Sr (42.7–53.7 ppm) but high Rb (81.1–100.0 ppm).

The Devonian monzogranite (samples L18M84I-V) has relatively high SiO_2 (65.8–68.4 wt%) and total alkali (6.3–8.0 wt%) contents, indicating the affinities of high-K calc-alkaline and calc-alkaline rocks (Fig. 6b). The low A/CNK values (0.9–1.0) imply metaluminous characteristics (Fig. 6c). Moreover, this monzogranite has variable REE contents (25.0–120 ppm) with weakly negative to strongly positive Eu anomalies (0.8–1.7), and is characterized by enrichment in LREEs and depletion in HREEs (Fig. 7e). The primitive mantle normalized spidergram displays significantly negative Nb, Ta, P and Ti anomalies and enrichment of Rb, Ba, Th and U (Fig. 7f).

The Devonian monzogranite (samples L18M69I-IV) has high SiO_2 (73.1–74.3 wt%), moderate Al_2O_3 (13.7–15.1 wt%) and CaO (1.5–1.8 wt %), showing calc-alkaline and weakly peraluminous characteristics (Fig. 6b and c). This monzogranite has weakly negative Eu anomalies (0.6–0.7) with enrichment in LREEs and depletion in HREEs (Fig. 7g). The primitive mantle normalized spidergram shows significantly negative Nb, Ta, P and Ti anomalies and enrichment of Rb, Ba, Zr and Hf (Fig. 7h).

The Devonian monzogranite (samples L19M82I-V) has similar SiO_2 (73.8–74.7 wt%) and MgO (0.3–0.4 wt%) as another monzogranite (L18M69I-IV), and is characterized by high-K calc-alkaline and weakly peraluminous features (Fig. 6b and c). This monzogranite has negative Eu anomalies (0.6–0.7) with enrichment in LREEs (Fig. 7i). Besides, this monzogranite shows significantly negative Nb, Ta, P and Ti anomalies in the primitive mantle normalized spidergram (Fig. 7j).

4.3. Whole-rock Sr-Nd and zircon Hf isotopes

The Ordovician K-feldspar granite (samples L18M44I-VII) shows negative $\varepsilon_{Nd}(t)$ values (−2.0 to −1.4) with two-stage Nd model ages of 1.3–1.4 Ga, and has low initial $^{87}Sr/^{86}Sr$ ratios of 0.6984–0.7000. This

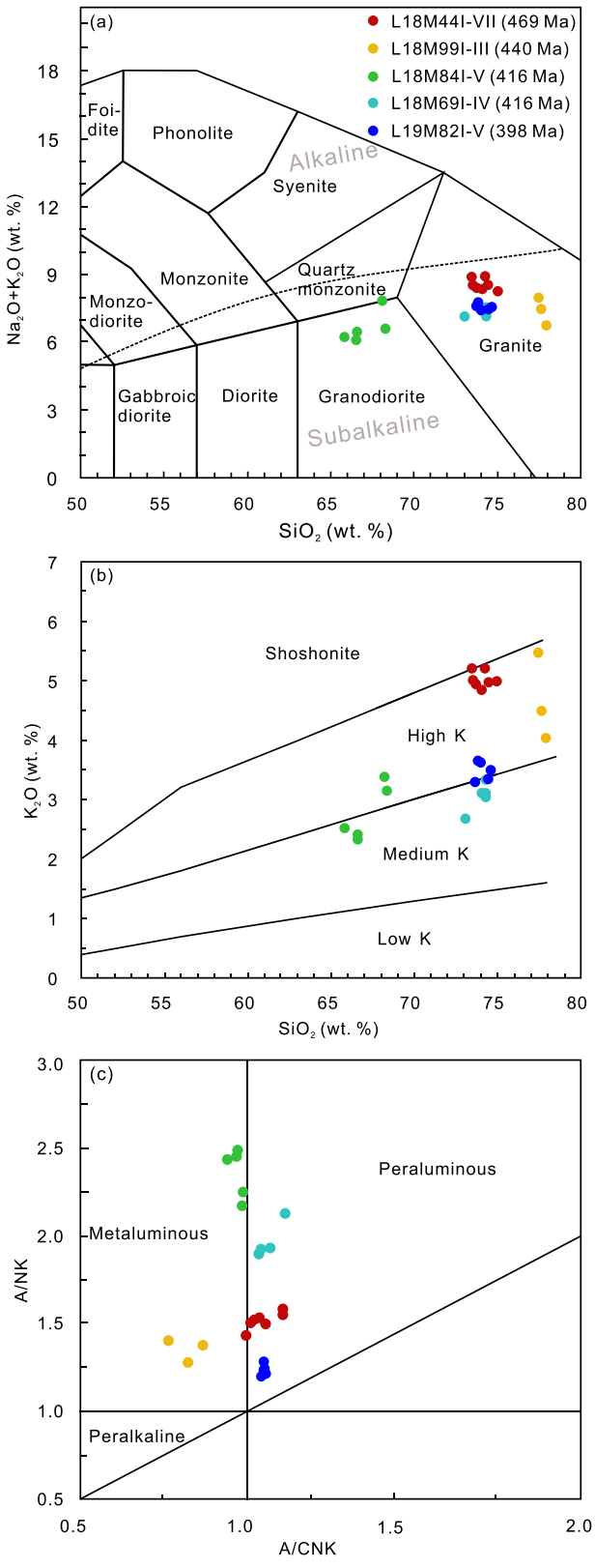

Fig. 6. Geochemical diagrams of granitic plutons. (a) Total alkali-silica (TAS) diagram (Le Bas et al., 1986); (b) SiO_2 versus K_2O diagram (Peccerillo and Taylor, 1976); (c) A/CNK versus A/NK diagram (Maniar and Piccoli, 1989).

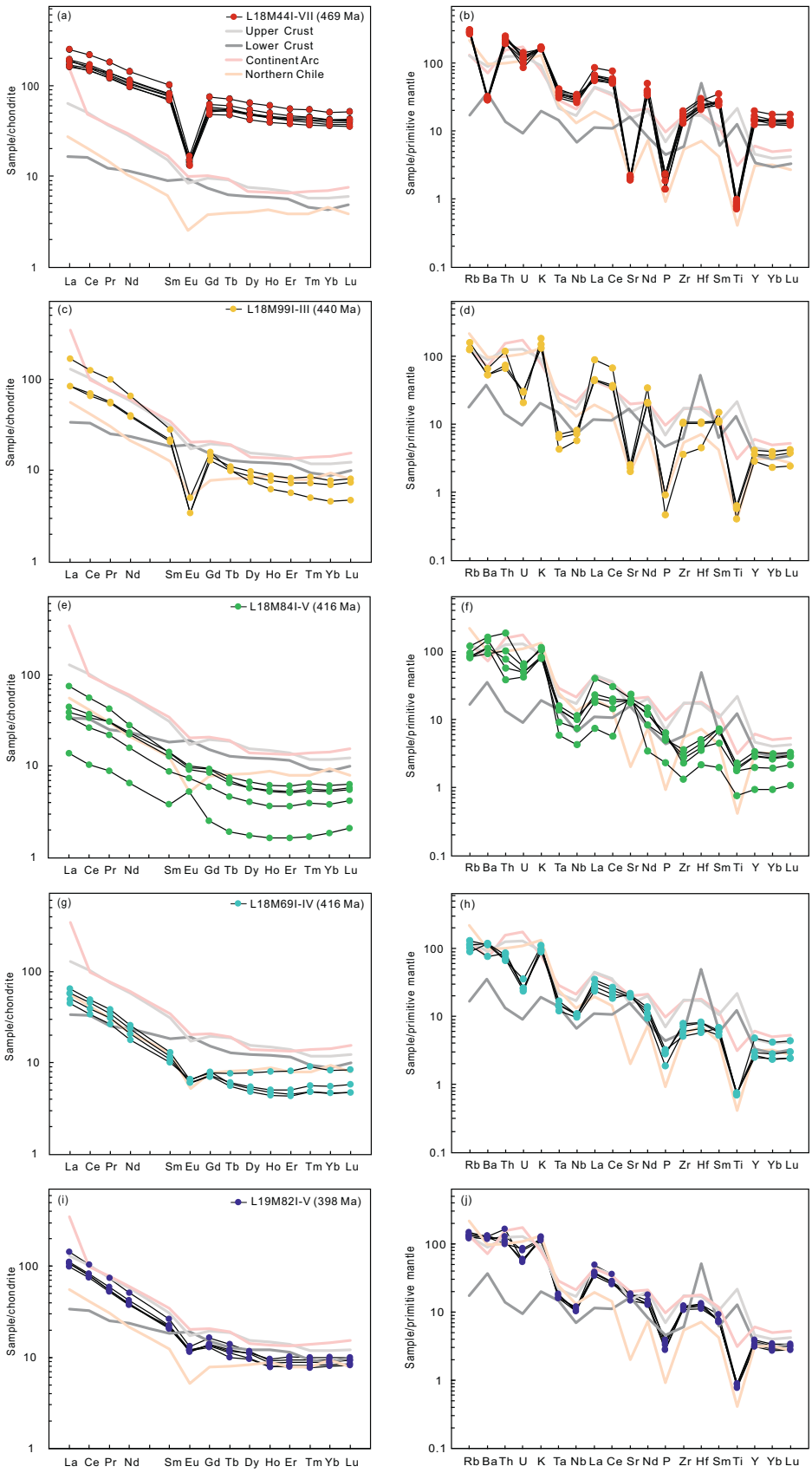

Fig. 7. Chondrite-normalized REE patterns and primitive-mantle normalized diagrams for granitic plutons. The data of the upper and lower crust are from Rudnick and Gao (2003). The data of the continent arc are from Drummond et al. (1996). The data of igneous rocks in the Northern Chile are from Coloma et al. (2017). Normalizing values are from Sun and McDonough (1989).

granite has positive zircon $\varepsilon_{Hf}(t)$ values (+1.4 to +5.0) with two-stage Hf model ages of 1.4–1.7 Ga.

The Silurian K-feldspar granite (samples L18M99I-III) has negative $\varepsilon_{Nd}(t)$ values (−4.7 to −4.4) with two-stage Nd model ages of 1.5–1.6 Ga, and shows variable zircon $\varepsilon_{Hf}(t)$ values (−2.6 to +2.8) with two-stage Hf model ages of 1.6–2.1 Ga. Specially, the Silurian K-feldspar granite has low initial $^{87}Sr/^{86}Sr$ ratios (0.6942–0.6953), which are similar to the Ordovician K-feldspar granites. Given that the uncertainty in I_{Sr} calculation for individual sample increases with increasing $^{87}Rb/^{86}Sr$ ratios, the induced errors in calculated I_{Sr} become too large to yield meaningful I_{Sr} values (Wu et al., 2000; Jahn et al., 2009). $^{87}Rb/^{86}Sr$ ratios for the Silurian and Ordovician K-feldspar granites (4.9564–13.0450) are large, and thus I_{Sr} values for these granites are not used in the subsequent discussion.

Three Devonian monzogranites (samples L18M84I-V, L18M69I-IV and L19M82I-V) display similar Sr and Hf isotopic features. They have low I_{Sr} values (0.7055–0.7067), and variable $\varepsilon_{Hf}(t)$ values (−2.1 to +5.5) that correspond to T_{DM2} ages of 1.3–2.0 Ga. The monzogranite (samples L18M84I-V) shows negative $\varepsilon_{Nd}(t)$ values from −4.4 to −4.2 (two-stage Nd model ages of ~1.5 Ga), while the other two monzogranites (samples L18M69I-IV and L19M82I-V) yield slightly negative $\varepsilon_{Nd}(t)$ values from −1.3 to +0.5 (two-stage Nd model ages of 1.1–1.3 Ga).

5. Discussion

5.1. Classification of Ordovician to Devonian granitic plutons

Chappell and White (1974) proposed the classification of I- and S-type granitic rocks, in which the A/CNK values of I-type granitic rocks are usually less than 1.1, and S-type granitic rocks show higher A/CNK values than I-type. A-type granitic rocks, which were proposed by Whalen et al. (1987), are characterized by high ratios of Ga/Al and high contents of Zr, Nb, Ce and Y. The Ordovician K-feldspar granite (samples L18M44I-VII) contains high 10000*Ga/Al (3.4–3.6) and high Zr + Nb + Ce + Y (329–446 ppm), showing the characteristics of A-type granitic rocks (Fig. 8a, b and c). In the A-type granite discrimination diagram (Eby, 1992), the Ordovician K-feldspar granites are plotted into the A_2-type field, implying the affinity of A_2-type granitic rocks (Fig. 8d). The other four plutons, including the Silurian K-feldspar granite (samples L18M99I-III) and three Devonian monzogranites (samples L18M84I-V, L18M69I-IV and L19M82I-V), fall into I- and S-type fields (Fig. 8a and b). Furthermore, these four plutons have low A/CNK values (0.8–1.1; Fig. 6c), making them akin to I-type granitic rocks.

5.2. Petrogenesis of the Ordovician to Devonian granitic plutons

All of five granitic plutons, including the Ordovician K-feldspar granite (samples L18M44I-VII), the Silurian K-feldspar granite (samples

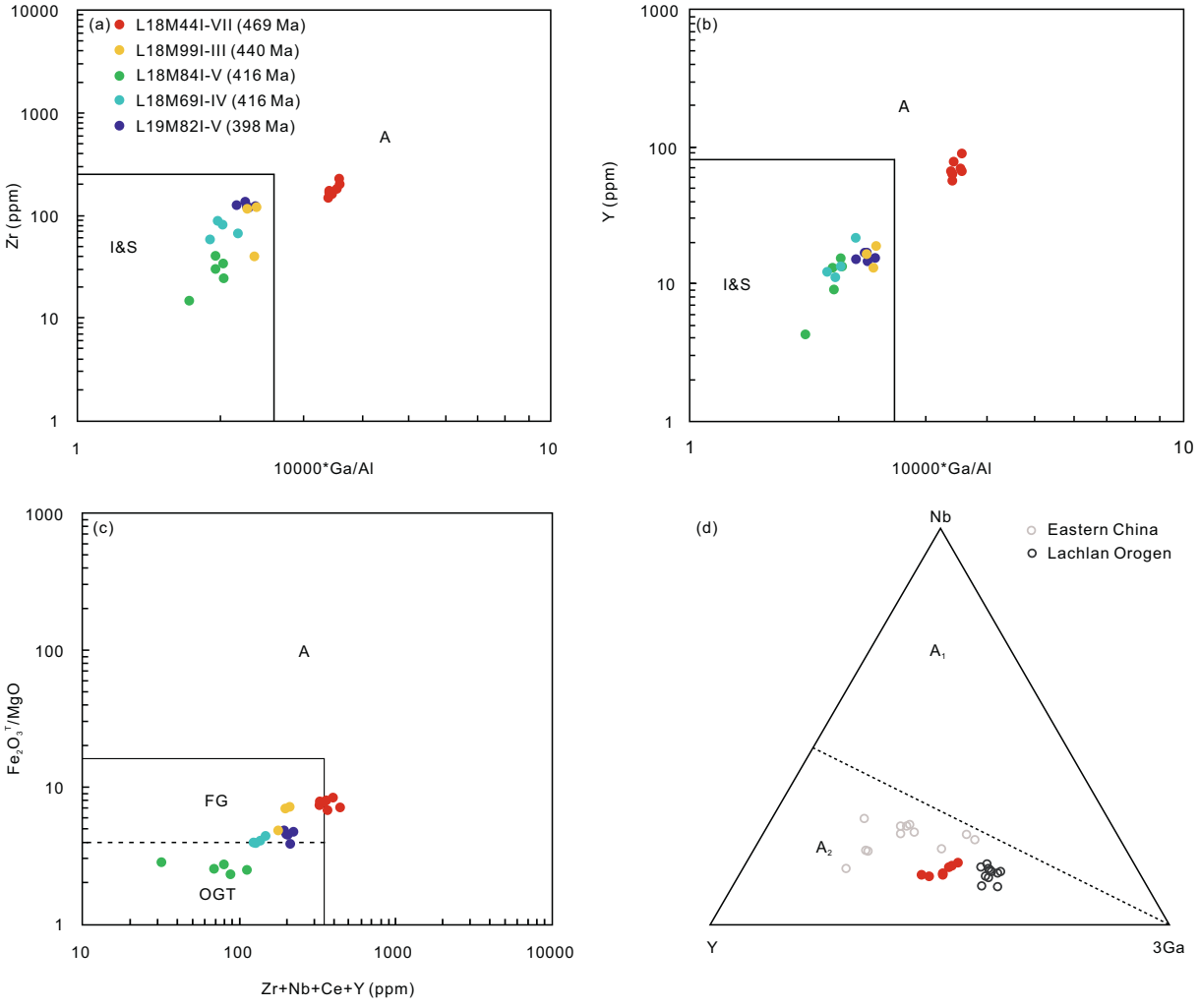

Fig. 8. (a) 10000*Ga/Al diagram versus Zr diagram; (b) 10000*Ga/Al diagram versus Y diagram; (c) Zr + Nb + Ce + Y versus $Fe_2O_3^T$/MgO diagram (Whalen et al., 1987); (d) Discriminating diagram for anorogenic (A_1) and post-orogenic (A_2) granitic rocks (Eby, 1992). The data of granitoids in Eastern China are from Sun et al. (2015). The data of granitic rocks in Eastern Australia are from Hergt et al. (2007).

L18M99I-III), and three Devonian monzogranites (samples L18M84I-V, L18M69I-IV and L19M82I-V), possess high SiO_2, low MgO, Cr and Ni contents (Table S3), implying a crustal origin (Rudnick and Gao, 2003). Available experimental studies show that partial melting of mafic rocks in the lower crust can generate calc-alkaline to high-K calc-alkaline felsic magmas (Roberts and Clemens, 1993). Five plutons in this study show calc-alkaline to high-K calc-alkaline characteristics (Fig. 6b), suggesting that mafic rocks in the lower crust might be the potential source of five plutons. Furthermore, dehydration melting of low-K basaltic rocks can produce the melts with low K_2O and high Na_2O/K_2O ratios (> 1; Rapp and Watson, 1995), whereas the K-rich melts with $Na_2O/K_2O < 1$ can be caused by dehydration melting of medium-to-high K basaltic rocks (Sisson et al., 2004). Both Ordovician and Silurian K-feldspar granites contain high K_2O (4.0–5.5 wt%) and low Na_2O/K_2O (0.46–0.73), which are similar as the partial melting of medium-to-high K basaltic rocks in the lower crust. In contrast, three Devonian monzogranites (samples L18M84I-V, L18M69I-IV and L19M82I-V) have relatively low K_2O (2.4–3.7 wt%) contents and high Na_2O/K_2O ratios (1.1–1.7), which are consistent with the dehydration melting of low-K basaltic rocks (Rapp and Watson, 1995). Isotopic data show narrow ranges of $\varepsilon_{Nd}(t)$ values (−4.7 to +0.5) and zircon $\varepsilon_{Hf}(t)$ values (−2.6 to +5.5) for these five granitic plutons, which plot between the evolutional lines of depleted mantle and the Precambrian basement in the Zavkhan, Tarvagatay and Baydrag blocks (Fig. 9). The Precambrian basement mainly contains Archean to Proterozoic tonalitic to granitic gneiss and granulite, which have much more negative $\varepsilon_{Nd}(t)$ and zircon $\varepsilon_{Hf}(t)$ values than five plutons in this study (Fig. 9), indicating that the Precambrian basement cannot be the major magma source of five plutons. Zhang et al. (2015b) reported ~547 Ma subduction-related mafic microgranular enclaves within the Baydrag block, which show the narrow ranges of Hf and Nd isotopic compositions ($\varepsilon_{Hf}(t)$: −3.5 to +2.6; $\varepsilon_{Nd}(t)$: −2.1 to −1.6). The $\varepsilon_{Nd}(t)$ and zircon $\varepsilon_{Hf}(t)$ values of five granitic plutons are close to the evolutional array of these microgranular enclaves (Fig. 9). We consider that these enclaves might represent one of potential source rocks for the granitic plutons in this study. The effect of the crustal assimilation on the granitic plutons in this study is likely limited, given the narrow ranges of Hf and Nd isotopic compositions of these plutons that differ from rather radiogenic Hf and Nd isotope of microcontinental blocks of Zavkhan, Tarvagatay and Baydrag (Fig. 9). According to Jahn et al. (2015), the granitic plutons affected by the assimilation of the old crust commonly show wide ranges in Nd and Hf isotopes, which is inconsistent with our Nd and Hf data.

The Ordovician and Silurian K-feldspar granites (samples L18M44I-VII and L18M99I-III) as well as two Devonian monzogranites (samples L18M69I-IV and L19M82I-V) contain high SiO_2 (73.1–77.9 wt%), total alkali (6.8–8.9 wt%) and low $Mg^{\#}$ (22.4–37.3), suggesting that the fractional crystallization played an important role in the primary magma evolution of these granites. This is supported by the fact that four granitic plutons are plotted into the fractionated granite field in the Zr + Nb + Ce + Y vs. $Fe_2O_3^T$/MgO diagram (Fig. 8c). Furthermore, both Ordovician and Silurian K-feldspar granites have strong Sr and Eu anomalies (Fig. 7a-d). The fractionation of K-feldspar can result in the strong Ba and Eu anomalies, while the fractionation of plagioclase could cause the strong Sr and Eu anomalies (Wu et al., 2003). Thus, we consider that the fractionation of plagioclase might play an important role in the evolutionary process of granitic magma for two Ordovician and Silurian K-feldspar granites. Moreover, two Devonian monzogranites (samples L18M69I-IV and L19M82I-V) show weakly negative Eu anomalies, suggesting the fractionation of plagioclase and/or K-feldspar. In contrast, another Devonian monzogranite (samples L18M84I-V) displays both negative and positive Eu anomalies (δEu = 0.8–1.7). The positive anomalies may result from cumulation of plagioclase and K-feldspar, which are consistent with enrichment in Sr and Ba for this Devonian monzogranite.

The Hf and Nd isotopes generally exhibit a good correlation during magmatic processes (Vervoort et al., 1999). However, three granitic plutons of the Ordovician K-feldspar granite (samples L18M44I-VII), the Silurian K-feldspar granite (samples L18M99I-III) and the Devonian monzogranite (samples L18M84I-V), have negative $\varepsilon_{Nd}(t)$ values (−4.7 to −1.5), but mostly positive $\varepsilon_{Hf}(t)$ values (−2.6 to +5.0), reflecting the Nd-Hf isotopic decoupling (Fig. 10). Several factors have been proposed to interpret the Nd-Hf isotopic decoupling, including the effect of garnet or zircon, as well as the inherited influence from the magma source during partial melting (Vervoort et al., 2000; Vervoort et al., 2011). Garnet is a HREEs-bearing mineral and has high Lu/Hf ratio, and thus magma with depletion in HREEs can be generated within the garnet stability field (Vervoort et al., 2000). Zircon is a major mineral that bears Zr and Hf and has a very low Lu/Hf ratio, and the remove of zircons could result in the depletion in Zr and Hf (Vervoort et al., 2000; Vervoort et al., 2011). Three plutons with Nd-Hf decoupling in this study have flat HREE patterns, and are enriched in Zr and Hf, thus excluding the possibility of garnet and zircon effect. Alternatively, we infer that the Nd-Hf isotopic decoupling can be inherited from the magma source during partial melting (Vervoort et al., 2000), which could result from the incorporation of the sediments into the magma source, leading to high Nd/Hf ratio in the melts (Hanyu et al., 2006; Todd et al., 2010). Indeed, our Nd and Hf isotopic data of three granitic plutons show high Nd/Hf ratios (4.9–33.7), and fall into mixing curves of depleted mantle (Salters

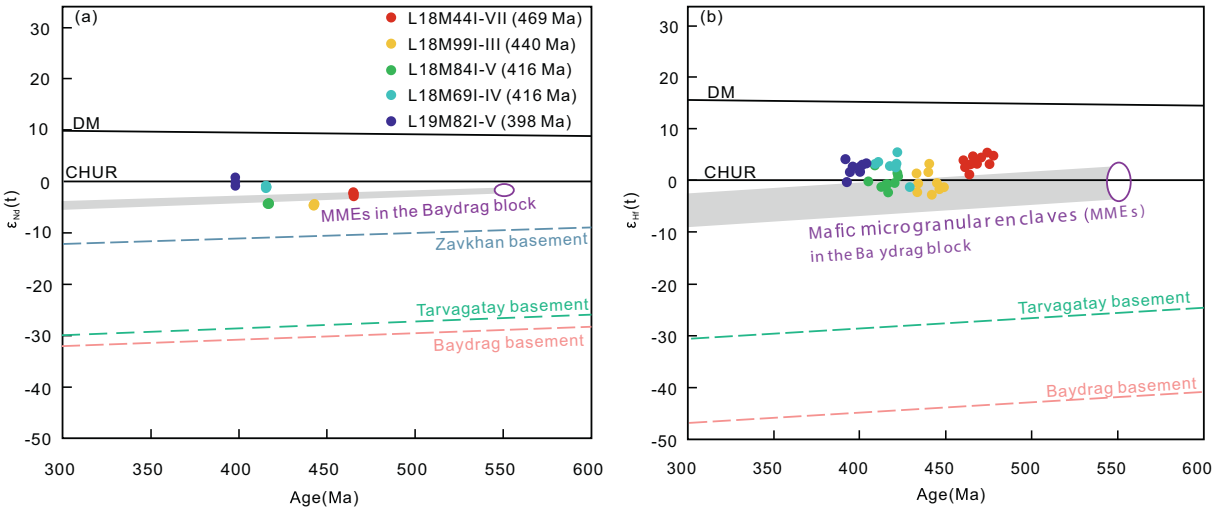

Fig. 9. Age versus $\varepsilon_{Nd}(t)$ and $\varepsilon_{Hf}(t)$ diagram. The isotopic data of MMEs (mafic microgranular enclaves) in (a) and (b) are from Zhang et al. (2015b). The isotopic data of the Precambrian blocks are from Kozakov et al. (2011, 2015) and Kröner et al. (2014, 2017) .

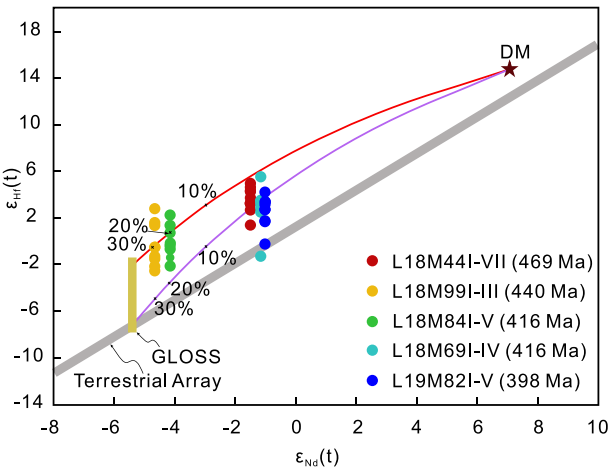

Fig. 10. The diagram of $\varepsilon_{Nd}(t)$ versus $\varepsilon_{Hf}(t)$ showing Nd-Hf decoupling of studied samples. The data of depleted mantle are from Salters and Stracke (2004). The subducted sediments are represented by the global subducting sediment (GLOSS; Plank and Langmuir, 1998). The Terrestrial Array is based on the formula ($\varepsilon_{Hf}(t) = 1.55 \times \varepsilon_{Nd}(t) + 1.21$) by Vervoort et al. (2011).

and Stracke, 2004) and the sediments represented by the global subducted sediment (GLOSS) (Fig. 10; Plank and Langmuir, 1998). We consider that the Nd-Hf decoupling of three plutons may have been inherited from their mafic source that was previously metasomatized by subduction sediments.

5.3. Tectonic implications

In the westernmost Mongol-Okhotsk Orogen (Hangay Range, Figs. 1 and 2), the Ediacaran to Cambrian magmatic rocks (~579–514 Ma) mainly occur along the northeastern margin of the Baydrag block (Fig. 2). These rocks are predominantly calc-alkaline or high-K calc-alkaline, and are characterized by depletion in Nb, Ta, P and Ti, suggesting a subduction-related origin (Demoux et al., 2009; Jahn et al., 2004; Zhang et al., 2015b). Farther east, the late Neoproterozoic to Cambrian accretionary complex was developed in the Bayanhongor zone that contains typical tectonic mélange with ~647–630 Ma ophiolitic rocks incorporated (Fig. 11; Buchan et al., 2001; Jian et al., 2010; Şengör et al., 2018). The coeval development of the accretionary complex with arc-related magmatic rocks farther west illustrates a roughly west-dipping subduction system (current coordinate) beneath the microcontinents of Baydrag, Zavkhan and Tarvagatay (Figs. 1b and 13a). The subduction remained active in the Ordovician given the occurrence of active marginal turbidite of the Zag zone (Narantsetseg et al., 2019), which is fault-bounded with the Bayanhongor zone to the west and the Hangay-Hentey complex to the east (Fig. 1c; Buchan et al., 2001; Osozawa et al., 2008), and likely represents a coherent sequence within the accretionary wedge (Şengör et al., 2018; Şengör et al., 1993). This is supported by geochemical features of the turbidite of the Zag zone, which shows an immature source and a deposition setting along the active margin (Narantsetseg et al., 2019). Our new results reveal that the Ordovician K-feldspar granite (samples L18M44I-VII) intruded into the Zag zone at 469 ± 3 Ma (Fig. 2, 5a and b). This age constrains the deposition of the Zag zone to be older than ~469 Ma. The Ordovician K-feldspar granite has high 10000*Ga/Al (3.4–3.6) and Zr + Nb + Ce + Y (329–446 ppm), similar to A-type granitic rocks (Fig. 8a and b). Generally, A-type granitic rocks form in an extensional geodynamic environment (Collins et al., 2019; Hergt et al., 2007). Eby (1992) subdivided A-type granitic rocks into two sub-types with A_1-type granitic rocks in anorogenic settings (continental rifts), and A_2-type granitic rocks in post-orogenic settings (post-collisional or back-arc extension). Our Ordovician K-feldspar granite belongs to A_2-type (Fig. 8d), similar to the A_2-type granite in Eastern China (Sun et al., 2015) and Eastern Australia (Lachlan Orogen) that has been attributed to the back-arc

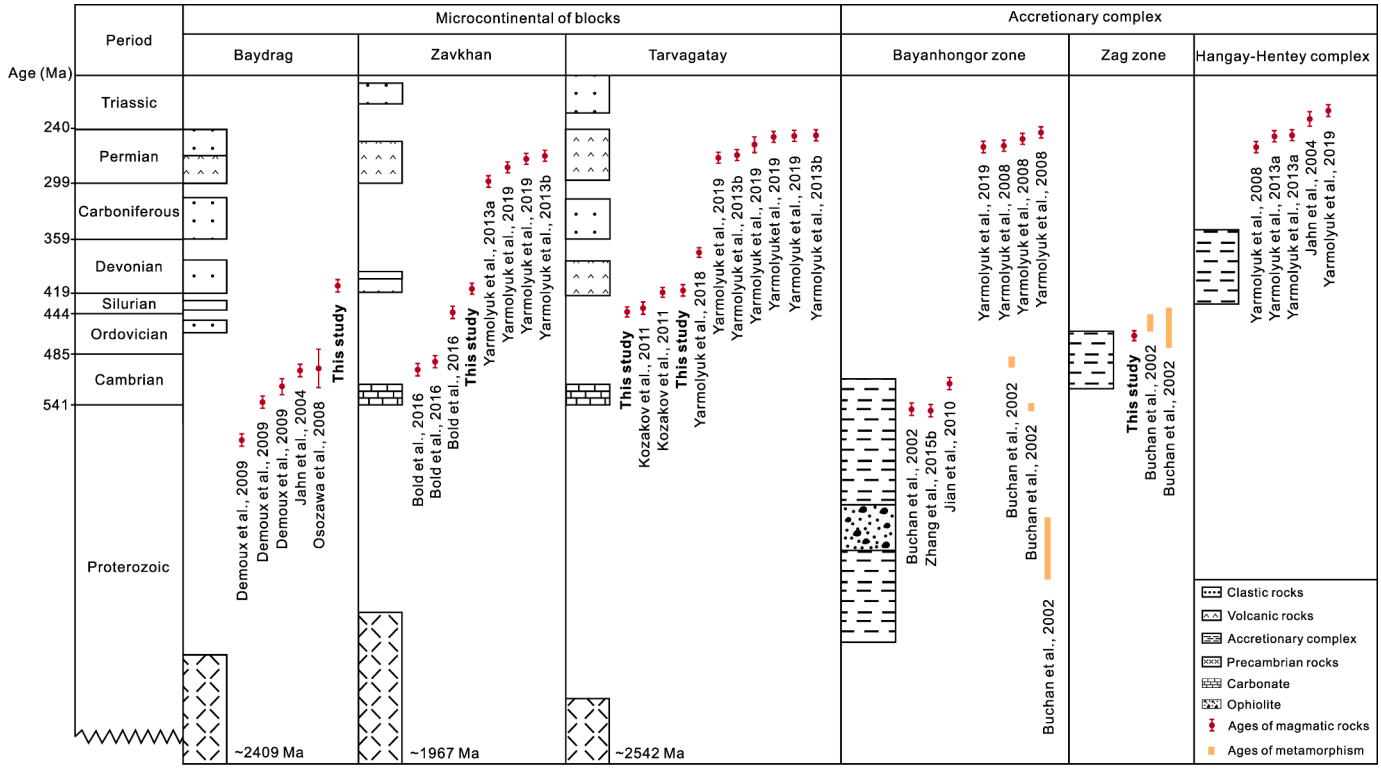

Fig. 11. Spatial and temporal diagram of the westernmost Mongol-Okhotsk Orogen (Hangay Range), which is after Badarch et al. (2002), Bold et al. (2016), Demoux et al. (2009), Kröner et al. (2014) and Li et al. (2019). The age data of granitoids can refer to Table S1.

extension in response to an episode of slab rollback of the subducted oceanic plate (Lachlan Orogen; Collins et al., 2019; Hergt et al., 2007). Furthermore, the Ordovician K-feldspar granite intruded into the accretionary complex of the Zag zone, indicating the retreat of the magmatic front towards the trench (Fig. 2). Therefore, we consider that the Ordovician K-feldspar granite was possibly generated in response to an episode of slab rollback (Fig. 13b). In Pearce diagrams, the Ordovician K-feldspar granite falls into the WPG (within plate granite) field, which is similar as A-type granitic rocks in the Lachlan Orogen (Eastern Australia) that were developed in a back-arc extensional setting associated with the slab rollback (Fig. 12; Collins et al., 1982; Collins et al., 2019; Hergt et al., 2007; King et al., 1997). In the eastern CAOB (NE China), the Ordovician A_2-type granite is alternatively interpreted to be associated with the collision of Songnen and Jiamusi blocks following the closure of the Paleo-Asian Ocean (Deng et al., 2018). This alternative interpretation is not preferred for Ordovician A_2-type K-feldspar granite in this study given that the collision of microcontinental blocks (around the Hangay Range, Fig. 1) with the Siberian margin occurred much earlier at ~630–610 Ma (Gladkochub et al., 2019).

The Silurian to Devonian granitic plutons (samples L18M99I-III, L18M84I-V, L18M69I-IV and L19M82I-V) in this study have calc-alkali or high-K calc-alkali characteristics, and belong to I-type granites. In Pearce diagrams, they fall into the VAG (volcanic arc granite) field (Fig. 12), manifesting an arc-related origin. Furthermore, they are characterized by enrichment in LILEs (e.g. Rb, K, Th) and depletion in HFSEs (e.g. Nb, Ta, P, Ti; Fig. 7), which are typical features of granitic rocks in active continental margins (Roberts and Clemens, 1993), such as magmatic rocks in northern Chile (Fig. 7; Coloma et al., 2017). These geochemical characteristics indicate that the Silurian to Devonian granitic plutons were probably developed within a magmatic arc (Fig. 13c). Similarly, Kozakov et al. (2011) and Yarmolyuk et al. (2018) reported the Silurian and Devonian diorites in the Tarvagatay block (Fig. 2; Table S1), and interpreted them to be formed in a supra-subduction zone given the enrichment of LILEs and depletion of HFSEs for these rocks. Spatially, the Silurian to Devonian granitic plutons intruded into the Tarvagatay, Zavkhan and Baydrag blocks, to the west of the Ordovician granitic pluton that was emplaced into the Zag zone (Fig. 2). This indicates that the subducted slab in the Silurian to Devonian might be relatively flatter, compared to the Ordovician subduction scenario (Fig. 13b, c). Geologically, the Silurian accretionary complex is not well preserved in the western Mongol-Okhotsk Orogen, but the Devonian to Carboniferous accretionary complex widely occurs and is represented by the Hangay-Hentey complex (Fig. 2). This complex contains thick turbidite mixed with the oceanic plate stratigraphy, and

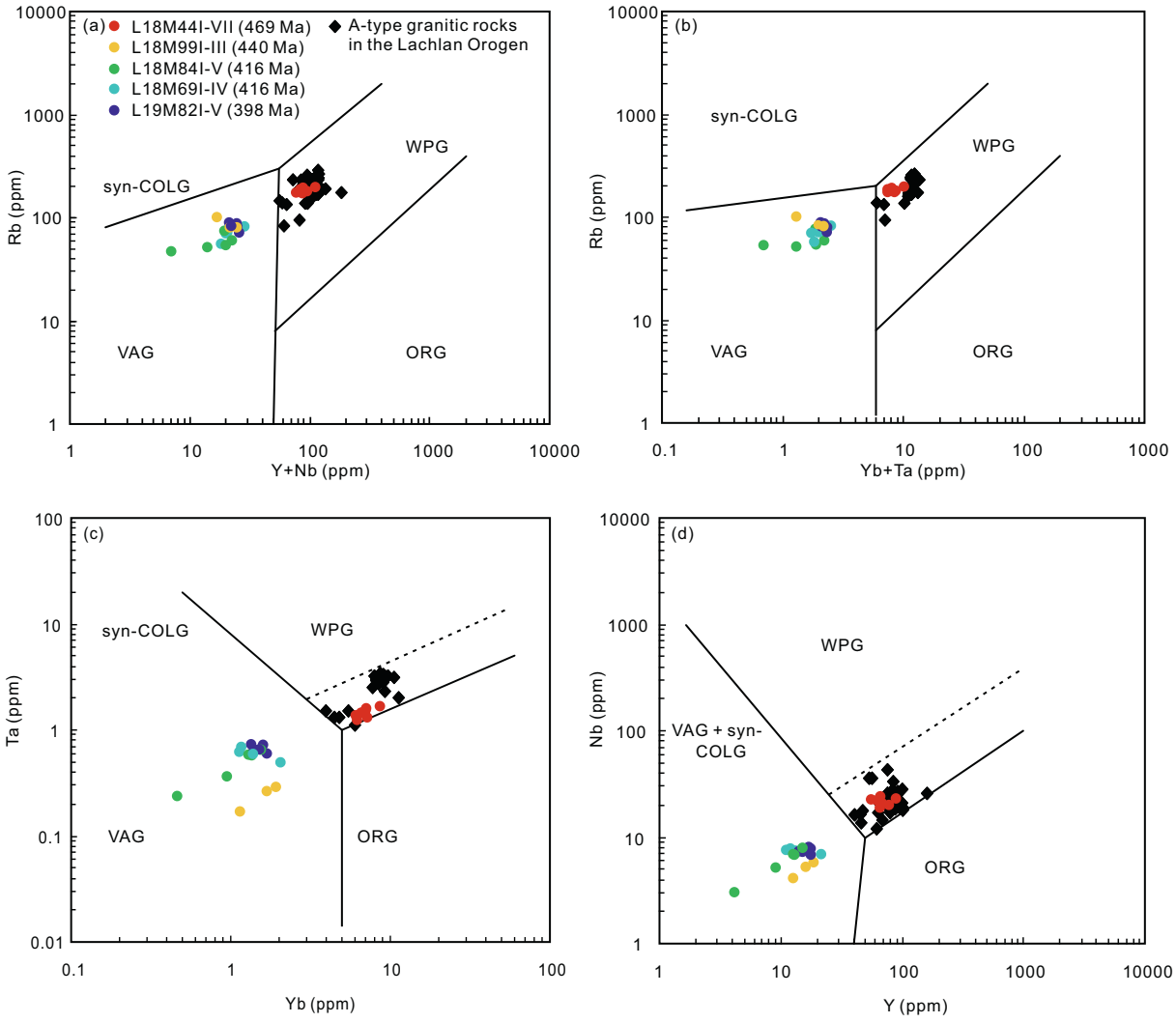

Fig. 12. Tectonic discrimination diagrams for Ordovician to Devonian granitic rocks in this study (Pearce et al., 1984). (a) Rb versus Y + Nb diagram, (b) Rb versus Yb + Ta diagram, (c) Ta versus Yb diagram, (d) Nb versus Y diagram. *Syn*-COLG: syn-collision granite; VAG: volcanic arc granite; ORG: ocean ridge granite; WPG: within plate granite. The data of A-type granitic rocks in the Lachlan Orogen (eastern Australia) are from Collins et al. (1982), Hergt et al. (2007), and King et al. (1997).

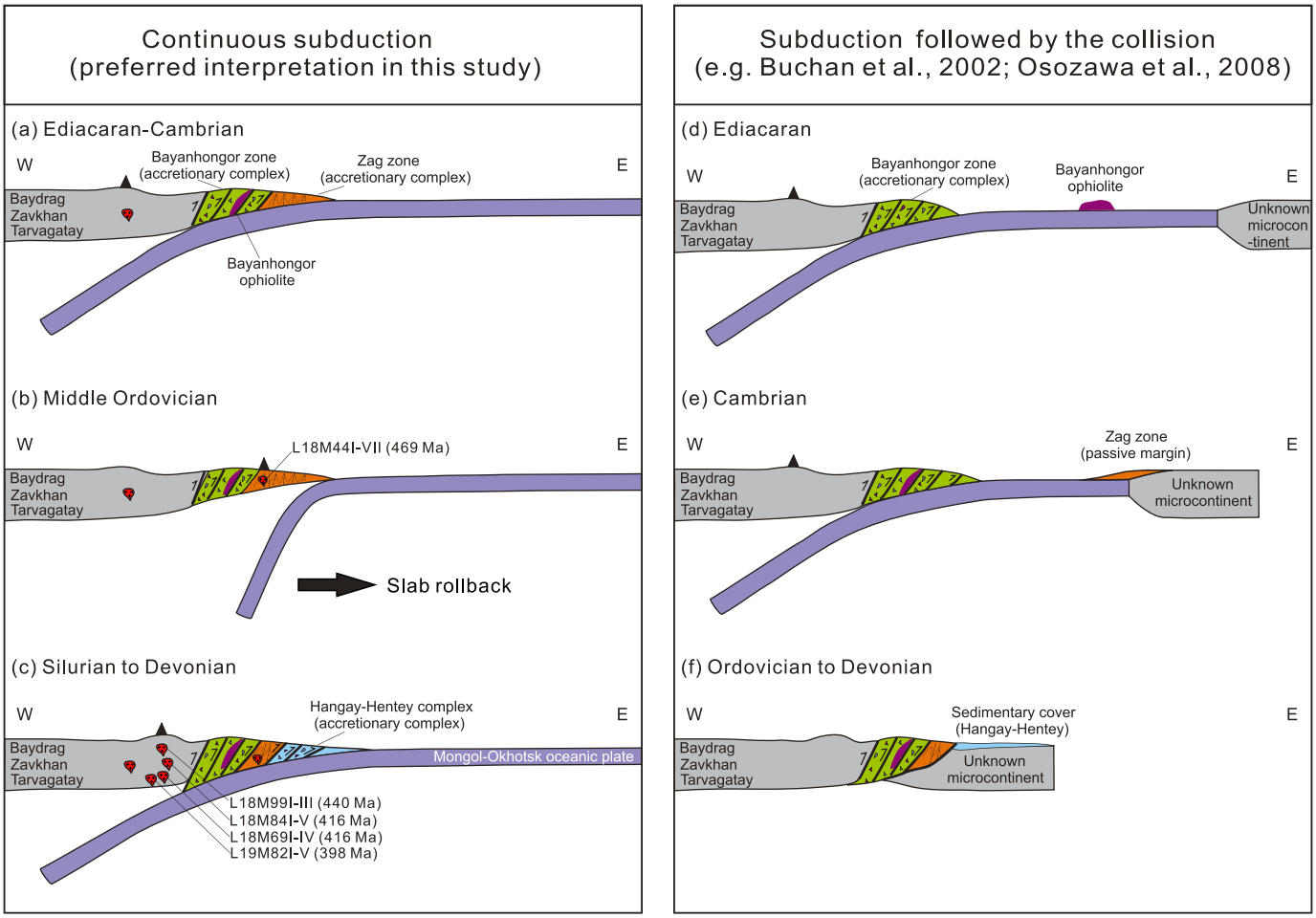

Fig. 13. Two alternative interpretations for the Ediacaran to Devonian tectonic evolution of the westernmost Mongol-Okhotsk Orogen, in which the continuous subduction model as indicated by Fig. 13a-c is preferred in this study. (a) The Andean-type subduction of the Mongol-Okhotsk oceanic plate in the Ediacaran-Cambrian. (b) An episode of slab rollback in the Middle Ordovician, as indicated by the occurrence of the A_2-type K-feldspar granite (samples L18M44I-VII) as well as the retreating of the magmatic front. (c) The continuous subduction of the Mongol-Okhotsk oceanic plate in the Silurian-Early Devonian, which was linked to the occurrence of Silurian-Early Devonian granitic plutons (samples L18M99I-III, L18M84I-V, L18M69I-IV and L19M82I-V). (d-f) Alternative tectonic model (Buchan et al., 2002; Osozawa et al., 2008), involving the Ediacaran to Cambrian subduction followed by a middle Paleozoic collision with an "unknown microcontinent" under the Hangay-Hentey complex, which is not supported by available data (see more discussion in the text).

shows typical block-in-matrix structures (Erdenesaihan et al., 2013; Tsukada et al., 2013), which, together with coeval arc-related magmatism reported in this study, defines an Andean-type arc-trench system (Fig. 13c).

In summary, our results show that the Ordovician to Devonian granitic plutons in the westernmost Mongol-Okhotsk Orogen (Hangay Range) are linked to the subduction that was likely initiated in the Ediacaran, consistent with the previous interpretation by Şengör et al., (2018) and Şengör et al. (1993). The oceanic basin associated with this subduction has been termed the Mongol-Okhotsk Ocean or the Hangay-Hentey Ocean (Delvaux et al., 1995; Şengör et al., 1993). On a larger scale, the Mongol-Okhotsk Orogen shows the curved oroclinal geometry in a map view (Figs. 1c and 2; Şengör et al., 1993), and oroclinal bending of this orogen was considered to occur in the Permian to Mesozoic (Li et al., 2022; van der Voo et al., 2015). Our newly-reported magmatic rocks are located in the hinge zone of the Mongolian Orocline, suggesting the active subduction beneath the hinge zone of the orocline in the early to middle Paleozoic. According to Şengör et al. (2018) and Şengör et al. (1993), the subduction was also active along two limbs of the orocline during this period. However, the pre-Devonian magmatic arc has not been recognized along two limbs of the orocline, and the earliest arc-related magmatic rocks that have been recognized are Devonian (Donskaya et al., 2013). Therefore, it remains enigmatic whether the subduction initiation was diachronous along different segments of the Mongolian Orocline.

Previous studies suggested an alternative interpretation for the Ordovician to Devonian tectonic evolution in the hinge area of the Mongolian Orocline (Hangay Range), which involves an early Paleozoic collisional event between the Baydrag/Zavkhan block and an "unknown microcontinent" beneath the Devonian to Carboniferous Hangay-Hentey complex (Fig. 13d-f; Buchan et al., 2002; Osozawa et al., 2008). However, there is no evidence for the existence of such a microcontinent beneath the Hangay-Hentey complex (Erdenesaihan et al., 2013; Ruppen et al., 2014; Tsukada et al., 2013). Furthermore, recent work interpreted that the Hangay-Hentey complex to represent a Devonian to Carboniferous accretionary complex given the juxtaposition of continent-derived turbidite and the oceanic plate stratigraphy as well as the typical block-in-matrix structures (Erdenesaihan et al., 2013; Tsukada et al., 2013). Therefore, an early Paleozoic collision is not supported by available data. Alternatively, a subduction-related model in the early to middle Paleozoic as shown in Fig. 13a-c is favored.

6. Conclusions

We reported new geochronological and geochemical data for five granitic plutons from the westernmost Mongol-Okhotsk Orogen in the Hangay Range (central Mongolia). The geochronological data display that five plutons yield Ordovician to Devonian ages, and are represented by the Ordovician K-feldspar granite (469 ± 3 Ma), the Silurian K-feldspar granite (440 ± 3 Ma) and three Devonian monzogranites (416 ± 4 Ma, 416 ± 4 Ma and 398 ± 4 Ma). The geochemical data show that all plutons have high SiO_2 (65.8–77.9 wt%) and total alkali (6.3–8.9 wt %) contents with Na_2O/K_2O ratios (0.5–1.7). The Ordovician K-feldspar granite belongs to A_2-type granite with high 10000*Ga/Al (3.4–3.6), while Silurian to Devonian granitic plutons are I-type granitoids with low A/CNK values (0.8–1.1). Five Ordovician to Devonian granitic plutons show relatively low $\varepsilon_{Nd}(t)$ (−4.7 to +0.5) and $\varepsilon_{Hf}(t)$ (−2.6 to +5.5). We interpreted five Ordovician to Devonian granitic plutons to be originated from partial melting of mafic rocks that were underplated in the lower crust in response to the Ediacaran to Cambrian subduction. The occurrence of these Ordovician to Devonian plutons was likely associated with the subduction of the Mongol-Okhotsk oceanic plate on a basis of their characteristics of depletion in Nb, Ti and Ta as well as the progressive development of accretionary complex in the study area. An episode of slab rollback may occur at ~469 Ma given A_2-type features of the Ordovician K-feldspar granite and spatial retreat of the magmatic front. We conclude that the subduction was likely active in the westernmost Mongol-Okhotsk Orogen in the early to middle Paleozoic.

Declaration of Competing Interest

The authors declare that they have no known competing financial interests or personal relationships that could have appeared to influence the work reported in this paper.

Acknowledgements

The study is financially supported by the international partnership program of the Chinese Academy of Sciences (132744KYSB20200001 and 132744KYSB20190039), the National Natural Science Foundation of China (42172237 and 42021002), Hong Kong Research Grant Council (HKU17302317), and a project from Guangdong Province (2019QN01H101). We thank Chutian Shu, Wei Li, Xinyu Wang, Shengling Sun, Shixi Cai and Xiangling Tu for help of experimental work, and Zhiwei Chen and Enkhdalai Batkhuyag for the assistance in the field. Yang Yu and Jinheng Liu are acknowledged for the discussion on the isotope geochemistry. The manuscript benefits from constructive comments from the Editor (Xian-Hua Li), Changzhou Deng, and an anonymous reviewer. This is a contribution of GIGCAS (No. IS- 3070), the Chemical Geodynamics Joint Laboratory between Hong Kong University and GIG (CAS) as well as IGCP 662.

Appendix A. Supplementary data

Supplementary data to this article can be found online at https://doi.org/10.1016/j.lithos.2021.106463.

References

Amelin, Y., Lee, D.-C., Halliday, A.N., Pidgeon, R.T., 1999. Nature of the Earth's earliest crust from hafnium isotopes in single detrital zircons. Nature 399, 252–255.
Badarch, G., Cunningham, W.D., Windley, B.F., 2002. A new terrane subdivision for Mongolia: implications for the Phanerozoic crustal growth of Central Asia. J. Asian Earth Sci. 21, 87–110.
Blichert-Toft, J., Albarede, F., 1997. The Lu-Hf geochemistry of chondrites and the evolution of the mantle-crust system. Earth Planet. Sci. Lett. 148, 243–253.
Bold, U., Crowley, J.L., Smith, E.F., Sambuu, O., Macdonald, F.A., 2016. Neoproterozoic to early Paleozoic tectonic evolution of the Zavkhan terrane of Mongolia: Implications for continental growth in the Central Asian orogenic belt. Lithosphere 8, 729–750.
Buchan, C., Cunningham, D., Windley, B.F., Tomurhuu, D., 2001. Structural and lithological characteristics of the Bayankhongor Ophiolite Zone, Central Mongolia. J. Geol. Soc. Lond. 158, 445–460.
Buchan, C., Pfanderb, J., Kroner, A., Brewer, T.S., Tomurtogoo, O., Tomurhuu, D., Cunningham, D., Windley, B.F., 2002. Timing of accretion and collisional deformation in the Central Asian Orogenic Belt: implications of granite geochronology in the Bayankhongor Ophiolite Zone. Chem. Geol. 192, 23–45.
Chappell, B.W., White, A.J.R., 1974. Two contrasting granite types. Pac. Geol. 8, 173–174.
Collins, W.J., Beams, S.D., White, A.J.R., Chappell, B.W., 1982. Nature and Origin of A-Type Granites with Particular Reference to Southeastern Australia. Contrib. Mineral. Petrol. 80, 189–200.
Collins, W.J., Huang, H.-Q., Bowden, P., Kemp, A.I.S., 2019. Repeated S-I-A-type granite trilogy in the Lachlan Orogen and geochemical contrasts with A-type granites in Nigeria: implications for petrogenesis and tectonic discrimination. Geol. Soc. Lond., Spec. Publ. 491, 53–76.
Coloma, F., Valin, X., Oliveros, V., Vásquez, P., Creixell, C., Salazar, E., Ducea, M.N., 2017. Geochemistry of Permian to Triassic igneous rocks from northern Chile (28°-30°15'S): Implications on the dynamics of the proto-Andean margin. Andean Geol. 44, 147–178.
Delvaux, D., Moeys, R., Stapel, G., Melnikov, A., Ermikov, V., 1995. Palaeostress reconstructions and geodynamics of the Baikal region, Central Asia, Part I. Palaeozoic and Mesozoic pre-rift evolution. Tectonophysics 252, 61–101.
Demoux, A., Kröner, A., Badarch, G., Jian, P., 2009. Zircon ages from the baydrag block and the bayankhongor ophiolite zone: time constraints on late neoproterozoic to cambrian subduction- and accretion-related magmatism in Central Mongolia. J. Geol. 117, 377–397.
Deng, C., Sun, D., Sun, G., Lv, C., Qin, Z., Ping, X., Li, G., 2018. Age and geochemistry of early Ordovician A-type granites in the Northeastern Songnen Block, NE China. Acta Geochim. 37 (6), 805–819.
Donskaya, T.V., Gladkochub, D.P., Mazukabzov, A.M., Ivanov, A.V., 2013. Late Paleozoic-Mesozoic subduction-related magmatism at the southern margin of the Siberian continent and the 150 million-year history of the Mongol-Okhotsk Ocean. J. Asian Earth Sci. 62, 79–97.
Drummond, M.S., Defant, M.J., Kepezhinskas, P.K., 1996. Petrogenesis of slab-derived trondhjemite-tonalite-dacite/adakite magmas. Trans. R. Soc. Edinb. Earth Sci. 87, 205–215.
Eby, G.N., 1992. Chemical subdivision of the A-type granitoids:Petrogenetic and tectonic implications. Geology 20, 641–644.
Erdenesaihan, G., Ishiwatari, A., Orolmaa, D., Arai, S., Tamura, A., 2013. Middle Paleozoic greenstones of the Hangay region, Central Mongolia: remnants of an accreted oceanic plateau and forearc magmatism. J. Mineral. Petrol. Sci. 108, 303–325.
Gladkochub, D.P., Donskaya, T.V., Stanevich, A.M., Pisarevsky, S.A., Zhang, S., Motova, Z.L., Mazukabzov, A.M., Li, H., 2019. U-Pb detrital zircon geochronology and provenance of Neoproterozoic sedimentary rocks in southern Siberia: New insights into breakup of Rodinia and opening of Paleo-Asian Ocean. Gondwana Res. 65, 1–16.
Griffin, W.L., Pearson, N.J., Elusive, E., Jackson, S.E., van Achtenberg, E., O'Reilly, S.Y., She, S.R., 2000. The Hf isotope composition of carbonic mantle: LAM-MC-ICPMS analysis of zircon megacrysts in kimberlites. Geochim. Cosmochim. Acta 64, 133–147.
Griffin, W.L., Wang, X., Jackson, S.E., Pearson, N.J., O'Reilly, S.Y., 2002. Zircon geochemistry and magma mixing, SE China: in situ analysis of Hf isotopes, Tonglu and Pingtan igneous complexes. Lithos 61, 237–269.
Hanyu, T., Tatsumi, Y., Nakai, S.i., Chang, Q., Miyazaki, T., Sato, K., Tani, K., Shibata, T., Yoshida, T., 2006. Contribution of slab melting and slab dehydration to magmatism in the NE Japan arc for the last 25 Myr: Constraints from geochemistry. Geochem. Geophys. Geosyst. 7, 1–29.
Hergt, J., Woodhead, J., Schofield, A., 2007. A-type magmatism in the Western Lachlan Fold Belt? A study of granites and rhyolites from the Grampians region, Western Victoria. Lithos 97, 122–139.
Jahn, B.M., Capdevila, R., Liu, D., Vernon, A., Badarch, G., 2004. Sources of Phanerozoic granitoids in the transect Bayanhongor-Ulaan Baatar, Mongolia: geochemical and Nd isotopic evidence, and implications for Phanerozoic crustal growth. J. Asian Earth Sci. 23, 629–653.
Jahn, B.M., Litvinovsky, B.A., Zanvilevich, A.N., Reichow, M., 2009. Peralkaline granitoid magmatism in the Mongolian–Transbaikalian Belt: Evolution, petrogenesis and tectonic significance. Lithos 113, 521–539.
Jahn, B.M., Valui, G., Kruk, N., Gonevchuk, V., Usuki, M., Wu, J.T.J., 2015. Emplacement ages, geochemical and Sr-Nd-Hf isotopic characterization of Mesozoic to early Cenozoic granitoids of the Sikhote-Alin Orogenic Belt, Russian Far East: Crustal growth and regional tectonic evolution. J. Asian Earth Sci. 111, 872–918.
Jian, P., Kröner, A., Windley, B.F., Shi, Y., Zhang, F., Miao, L., Tomurhuu, D., Zhang, W., Liu, D., 2010. Zircon ages of the Bayankhongor ophiolite mélange and associated rocks: Time constraints on Neoproterozoic to Cambrian accretionary and collisional orogenesis in Central Mongolia. Precambrian Res. 177, 162–180.
Jiang, Y., Sun, M., Zhao, G., Yuan, C., Xiao, W., Xia, X., Long, X., Wu, F., 2011. Precambrian detrital zircons in the early Paleozoic Chinese Altai: their provenance and implications for the crustal growth of Central Asia. Precambrian Res. 189, 140–154.
King, P.L., White, A.J.R., Chappell, B.W., Allen, C.M., 1997. Characterization and Origin of Aluminous A-type Granites from the Lachlan Fold Belt, Southeastern Australia. J. Petrol. 38, 371–391.
Kozakov, I.K., Kozlovsky, A.M., Yarmolyuk, V.V., Kovach, V.P., Bibikova, E.V., Kirnozova, T.I., Plotkina, Y.V., Zagornaya, N.Y., Fugzan, M.M., Erdenejargal, C.,

Lebedev, V.I., Eenjin, G., 2011. Crystalline complexes of the Tarbagatai block of the early Caledonian superterrane of Central Asia. Petrology 19, 426–444.
Kozakov, I.K., Kovach, V.P., Bibikova, E.V., Kirnozova, T.I., Lykhin, D.A., Plotkina, Y.V., Tolmacheva, E.V., Fugzan, M.M., Erdenezhargal, C., 2014. Late Riphean episode in the formation of crystalline rock complexes in the Dzabkhan microcontinent: Geological, geochronologic, and Nd isotopic-geochemical data. Petrology 22, 480–506.
Kozakov, I.K., Kirnozova, T.I., Kovach, V.P., Terent'eva, L.B., Tolmacheva, E.V., Fugzan, M.M., Erdenezhargal, C., 2015. Late Riphean age of the crystalline basement of the carbonate cover of the Dzabkhan microcontinent. Stratigr. Geol. Correl. 23, 237–245.
Kravchinsky, V.A., Sklyarov, E.V., Gladkochub, D.P., Harber, W.P., 2010. Paleomagnetism of the Precambrian Eastern Sayan rocks: implications for the Ediacaran-early Cambrian paleogeography of the Tuva-Mongolian composite terrane. Tectonophysics 486, 65–80.
Kröner, A., Kovach, V.P., Kozakov, I.K., Kirnozova, T., Azimov, P., Wong, J., Geng, H.Y., 2014. Zircon ages and Nd-Hf isotopes in UHT granulites of the Ider complex: a cratonic terrane within the Central Asian Orogenic Belt in NW Mongolia. Gondwana Res. 27, 1392–1406.
Kröner, A., Kovach, V., Kozakov, I., Aranovich, L., Xie, H., Tolmacheva, E., Kirnozova, T., Fuzgan, M., Serebryakov, N., Wang, K.-L., Lee, H.-Y., 2017. Granulites and Palaeoproterozoic lower crust of the Baidarik Block, Central Asian Orogenic Belt of NW Mongolia. J. Asian Earth Sci. 145, 393–407.
Le Bas, M.J., Le Maitre, R.W., Streckeisen, A., Zanettin, B., 1986. A chemical classification of volcanic rocks based on the total alkali-silica diagram. Petrology 27, 745–750.
Lehmann, J., Schulmann, K., Lexa, O., Corsini, M., Kroner, A., Stipska, P., Tomurhuu, D., Otgonbator, D., 2010. Structural constraints on the evolution of the Central Asian Orogenic Belt in SW Mongolia. Am. J. Sci. 310, 575–628.
Li, J., Tang, S.H., Zhu, X.K., Pan, C.X., 2017. Production and certification of the reference material GSB 04-3258-2015 as a $^{143}Nd/^{144}Nd$ isotope ratio reference. Geostand. Geoanal. Res. 41, 255–262.
Li, P., Sun, M., Shu, C., Yuan, C., Jiang, Y., Zhang, L., Cai, K., 2019. Evolution of the Central Asian orogenic belt along the Siberian margin from Neoproterozoic-early Paleozoic accretion to Devonian trench retreat and a comparison with Phanerozoic eastern Australia. Earth Sci. Rev. 198, 1–21.
Li, P., Sun, M., Narantsetseg, T., Jourdan, F., Hu, W., Yuan, C., 2022. First structural observation around the hinge of the Mongolian Orocline (Central Asia): implications for the geodynamics of oroclinal bending and the evolution of the Mongol-Okhotsk Ocean. Geol. Soc. Am. Bull. (in press).
Li, X.H., Zhou, H., Chung, S.L., Lo, C.H., Wei, G., Liu, Y., Lee, C.Y., 2002. Geochemical and Sr-Nd isotopic characteristics of late Paleogene ultrapotassic magmatism in southeastern Tibet. Int. Geol. Rev. 44, 559–574.
Li, X.H., Li, Z.X., Wingate, M.T.D., Chung, S.L., Liu, Y., Lin, G.C., Li, W.X., 2006. Geochemistry of the 755Ma Mundine well dyke swarm, northwestern Australia: part of a Neoproterozoic mantle superplume beneath Rodinia? Precambrian Res. 146, 1–15.
Liu, Y.S., Hu, Z.C., Gao, S., Günther, D., Xu, J., Gao, C.G., Chen, H.H., 2008. In situ analysis of major and trace elements of anhydrous minerals by LA-ICP-MS without applying an internal standard. Chem. Geol. 257, 34–43.
Ludwig, K.R., 2003. ISOPLOT 3.00: A Geochronological Toolkit for Microsoft Excel, 133. Berkeley Geochronology Center, California, Berkeley, pp. 391–402.
Maniar, P.D., Piccoli, P.M., 1989. Tectonic discrimination of granitoids. Geol. Soc. Am. Bull. 101, 635–643.
Narantsetseg, T., Oyunchimeg, T., Otgonbaatar, D., Tomurchudur, C., Li, P., Orolmaa, D., 2019. Depositional age and provenance of the Zag Formation. Explorer 60, 75–87 (in Mongolia with the English Abstract).
Nemchin, A.A., Cawood, P.A., 2005. Discordance of the U–Pb system in detrital zircons: Implication for provenance studies of sedimentary rocks. Sediment. Geol. 182, 143–162.
Osozawa, S., Tsolmon, G., Majigsuren, U., Sereenen, J., Niitsuma, S., Iwata, N., Pavlis, T., Jahn, B.-M., 2008. Structural evolution of the Bayanhongor region, west-Central Mongolia. J. Asian Earth Sci. 33, 337–352.
Pearce, J., Harris, N.B.W., Tindle, A.G., 1984. Trace element discrimination diagrams for the Tectonic Interpretation of Granitic Rocks. J. Petrol. 25, 956–983.
Peccerillo, A., Taylor, S.R., 1976. Geochemistry of Eocene calc-alkaline volcanic rocks from the Kastamonu area, northern Turkey. Contrib. Mineral. Petrol. 58, 63–81.
Plank, T., Langmuir, C.H., 1998. The chemical composition of subducting sediment and its consequences for the crust and mantle. Chem. Geol. 145, 325–394.
Rapp, R.P., Watson, E.B., 1995. Dehydration melting of metabasalt at 8-32 kbar: implications for continental growth and crust-mantle recycling. J. Petrol. 26, 891–931.
Roberts, M.P., Clemens, J.D., 1993. Origin of high-potassium, talc-alkaline, I-type granitoids. Geology 21, 825–828.
Rudnick, R.L., Gao, S., 2003. Composition of the continental crust. Treat. Geochem. 3, 1–51.
Ruppen, D., Knaf, A., Bussien, D., Winkler, W., Chimedtseren, A., von Quadt, A., 2014. Restoring the Silurian to Carboniferous northern active continental margin of the Mongol-Okhotsk Ocean in Mongolia: Hangay-Hentey accretionary wedge and seamount collision. Gondwana Res. 25, 1517–1534.
Salters, V.J.M., Stracke, A., 2004. Composition of the depleted mantle. Geochem. Geophys. Geosyst. 5, 1–27.
Segal, I., Halicz, L., Platzner, I.T., 2003. Accurate isotope ratio measurements of ytterbium by multiple collection inductively coupled plasma mass spectrometry applying erbium and hafnium in an improved double external normalization procedure. J. Anal. At. Spectrom. 18, 1217–1223.
Şengör, A.M.C., Natal'in, B.A., Burtman, V.S., 1993. Evolution of the Altaid tectonic collage and Palaeozoic crustal growth in Eurasia. Nature 364, 299–307.
Şengör, A.M.C., Natal'in, B.A., Sunal, G., van der Voo, R., 2018. The Tectonics of the Altaids: Crustal Growth during the Construction of the Continental Lithosphere of Central Asia between ~750 and ~130 Ma Ago. Annu. Rev. Earth Planet. Sci. 46, 439–494.
Sisson, T.W., Ratajeski, K., Hankins, W.B., Glazner, A.F., 2004. Voluminous granitic magmas from common basaltic sources. Contrib. Mineral. Petrol. 148, 635–661.
Sun, D.Y., Gou, J., Wang, T.H., Ren, Y.S., Liu, Y.J., Guo, H.Y., Liu, X.M., Hu, Z.C., 2013. Geochronological and geochemical constraints on the Erguna massif basement, NE China-subduction history of the Mongol-Okhotsk oceanic crust. Int. Geol. Rev. 55, 1801–1816.
Sun, F., Xu, X., Zou, H., Xia, Y., 2015. Petrogenesis and magmatic evolution of ~130 Ma A-type granites in Southeast China. J. Asian Earth Sci. 98, 209–224.
Sun, S.S., McDonough, W.F., 1989. Chemical and isotopic systematics of oceanic basalts: implications for mantle composition and processes. Geol. Soc. Lond., Spec. Publ. 42, 313–345.
Tanaka, T., Togashi, S., Kamioka, H., Amakawa, H., Kagami, H., Hamamoto, T., 2000. Jndi-1: a neodymium isotopic reference in consistency with lajolla neodymium. Chem. Geol. 168, 279–281.
Thirlwall, M.F., 1991. Long-term reproducibility of multicollector sr and nd isotope ratio analysis. Chem. Geol. 94, 85–104.
Todd, E., Gill, J.B., Wysoczanski, R.J., Handler, M.R., Wright, I.C., Gamble, J.A., 2010. Sources of constructional cross-chain volcanism in the southern Havre Trough: New insights from HFSE and REE concentration and isotope systematics. Geochem. Geophys. Geosyst. 11, 1–31.
Tsukada, K., Nakane, Y., Yamamoto, K., Kurihara, T., Otoh, S., Kashiwagi, K., Chuluun, M., Gonchigdorj, S., Nuramkhaan, M., Niwa, M., Tokiwa, T., 2013. Geological setting of basaltic rocks in an accretionary complex, Khangai-Khentei Belt, Mongolia. Island Arc 22, 227–241.
van der Voo, R., van Hinsbergen, D.J.J., Domeier, M., Spakman, W., Torsvik, T.H., 2015. Latest Jurassic-earliest cretaceous closure of the Mongol-Okhotsk Ocean: a paleomagnetic and seismological-tomographic analysis. Geol. Soc. Am. Spec. Paper 513, 589–606.
Vervoort, J.D., Patchett, P.J., Blichert-Toft, J., Albare'de, F., 1999. Relationships between Lu-Hf and Sm-Nd isotopic systems in the global sedimentary system. Earth Planet. Sci. Lett. 168, 79–99.
Vervoort, J.D., Patchett, P.J., Albarède, F., Blichert-Toft, J., Rudnick, R., Downes, H., 2000. Hf-Nd isotopic evolution of the lower crust. Earth Planet. Sci. Lett. 181, 115–129.
Vervoort, J.D., Plank, T., Prytulak, J., 2011. The H-Nd isotopic composition of marine sediments. Geochim. Cosmochim. Acta 75, 5903–5926.
Whalen, J.B., Currie, K.L., Chappell, B.W., 1987. A-type granites: geochemical characteristics, discrimination and petrogenesis. Contrib. Mineral. Petrol. 95, 407–419.
Windley, B.F., Alexeiev, D., Xiao, W., Kröner, A., Badarch, G., 2007. Tectonic models for accretion of the Central Asian Orogenic Belt. J. Geol. Soc. 164, 31–47.
Wu, F.Y., Jahn, B.M., Wilde, S., Sun, D.Y., 2000. Phanerozoic crustal growth: U±Pb and Sr±Nd isotopic evidence from the granites in northeastern China. Tectonophysics 328, 89–113.
Wu, F.Y., Jahn, B.M., Wilde, S.A., Lo, C.H., Yui, T.F., Lin, Q., Ge, W.C., Sun, D.Y., 2003. Highly fractionated I-type granites in NE China (I): geochronology and petrogenesis. Lithos 66, 241–273.
Wu, F.Y., Yang, Y.H., Xie, L.W., Yang, J.H., Xu, P., 2006. Hf isotopic compositions of the standard zircons and baddeleyites used in U-Pb geochronology. Chem. Geol. 234 (1–2), 105–126.
Xiao, W.J., Windley, B.F., Sun, S., Li, J., Huang, B., Han, C., Yuan, C., Sun, M., Chen, H., 2015. A tale of amalgamation of three permo-triassic collage systems in Central Asia: oroclines, sutures, and terminal accretion. Annu. Rev. Earth Planet. Sci. 43, 477–507.
Yarmolyuk, V.V., Kozakov, I.K., Kozlovsky, A.M., Kudryashova, E.A., Travin, A.V., Kirnozova, T.I., Fugzan, M.M., Plotkina, Y.V., 2018. The early Paleozoic active margin of the Khangai Segment of the Mongol-Okhotsk Ocean. Dokl. Earth Sci. 480, 559–563.
Yarmolyuk, V.V., Kozlovsky, A.M., Travin, A.V., Kozakov, I.K., Plotkina, Y.V., Eenjin, G., Kirnozova, T.I., Oyunchimeg, T., Fugzan, M.M., Sviridova, O.E., 2019. Duration and geodynamic nature of giant Central Asian Batholiths: geological and geochronological studies of the Khangai Batholith. Stratigr. Geol. Correl. 27, 73–94.
Zhang, L., Ren, Z.Y., Xia, X.P., Li, J., Zhang, Z.F., 2015a. IsotopeMaker: a Matlab program for isotopic data reduction. Int. J. Mass Spectrom. 392, 118–124.
Zhang, Y.Y., Sun, M., Yuan, C., Xu, Y.G., Long, X.P., Tomurhuu, D., Wang, C.Y., He, B., 2015b. Magma mixing origin for high Ba-Sr granitic pluton in the Bayankhongor area, Central Mongolia: response to slab roll-back. J. Asian Earth Sci. 113, 353–368.
Zorin, Y.A., Belichenko, V.G., Turutanov, E.K., Kozhevnikov, V.M., Ruzhentsev, S.V., Dergunov, A.B., Filippova, I.B., Tomurtogoo, E.K., Arvisbaatar, N., Bayasgalan, T., Biambaa, C., Khosbayar, P., 1993. The South Siberia-Central Mongolia transect. Tectonophysics 225, 361–378.